

Stability Enhancement of CsPbBr₃ Quantum Dots by Coating TiO₂ as a Surface
Encapsulation



A Thesis Submitted in Partial Fulfillment of the Requirements
for the Degree of Master of Engineering in Chemical Engineering

Department of Chemical Engineering

FACULTY OF ENGINEERING

Chulalongkorn University

Academic Year 2020

Copyright of Chulalongkorn University



จุฬาลงกรณ์มหาวิทยาลัย
CHULALONGKORN UNIVERSITY

การเพิ่มเสถียรภาพของ CsPbBr₃ ควอนตัมดอทโดยการเคลือบผิวด้วยไททานเนียมไดออกไซด์



วิทยานิพนธ์นี้เป็นส่วนหนึ่งของการศึกษาตามหลักสูตรปริญญาวิศวกรรมศาสตรมหาบัณฑิต

สาขาวิชาวิศวกรรมเคมี ภาควิชาวิศวกรรมเคมี
คณะวิศวกรรมศาสตร์ จุฬาลงกรณ์มหาวิทยาลัย

ปีการศึกษา 2563

ลิขสิทธิ์ของจุฬาลงกรณ์มหาวิทยาลัย

ปริณาม์ หนูเกตุ : การเพิ่มเสถียรภาพของ CsPbBr₃ ควอนตัมดอทโดยการเคลือบผิวด้วยไททาเนียมไดออกไซด์. (Stability Enhancement of CsPbBr₃ Quantum Dots by Coating TiO₂ as a Surface Encapsulation) อ.ที่ปรึกษาหลัก : ผศ. ดร.ปารวี วาศน์
 อำนวย, อ.ที่ปรึกษาร่วม : ศ.เทสุย่า คิตา

ซีเซียมเลดโบรไมด์ควอนตัมดอท (CsPbBr₃ QDs) เป็นวัสดุกึ่งตัวนำที่ได้รับความสนใจอย่างมากทั้งในแวดวงอุปกรณ์อิเล็กทรอนิกส์ และเซลล์ไฟฟ้าเคมีทางแสง เนื่องจากคุณสมบัติทางแสงที่ยืดหยุ่น อย่างไรก็ตาม ความเสถียรของวัสดุชนิดนี้ต่อปัจจัยทางสิ่งแวดล้อมยังคงเป็นอุปสรรคต่อการผลิตในระดับอุตสาหกรรม งานวิจัยนี้จึงได้เสนอกระบวนการเคลือบผิวแบบใหม่สำหรับ CsPbBr₃ QDs เพื่อป้องกันการรวมตัวของอนุภาค และเพิ่มเสถียรภาพของ CsPbBr₃ QDs โดยไม่ใช้กรรมวิธีทางความร้อนที่อุณหภูมิสูง หรือที่เรียกว่าวิธี in-situ ในที่นี้ ไททาเนียมเตตระไฮดรอกไซด์ซึ่งเป็นสารตั้งต้นสำหรับไททาเนียมไดออกไซด์ (TiO₂) หรือสารเคลือบผิว ได้ถูกฉีดเข้าไปในระบบระหว่างการก่อตัวของ CsPbBr₃ QDs เพื่อศึกษาผลของอุณหภูมิที่ทำการฉีดสารตั้งต้น ตั้งแต่ช่วง 25 ถึง 170 องศาเซลเซียส ต่อคุณสมบัติทางสัณฐานวิทยา โครงสร้าง และคุณสมบัติทางแสง ของ CsPbBr₃/TiO₂ ซึ่งถูกเตรียมด้วยวิธี in-situ และทำการเปรียบเทียบกับวิธี ex-situ ซึ่งเป็นวิธีเดิมที่ใช้ในการศึกษาที่ผ่านมา จากผลสรุปพบว่า นอกจากวิธี in-situ จะสามารถป้องกันการรวมตัวของอนุภาคแล้ว CsPbBr₃/TiO₂ ที่ถูกเคลือบ ณ อุณหภูมิ 25 องศาเซลเซียส ยังมีความเสถียรต่อแสง อากาศในบรรยากาศ ตัวทำละลายไม่มีขั้ว เช่น โทลูอิน และตัวทำละลายมีขั้ว เช่น น้ำ เนื่องมาจากการปกป้องของ TiO₂ บนพื้นผิวของ CsPbBr₃ QDs และโครงสร้างที่สมบูรณ์ของ CsPbBr₃ QDs หลังกระบวนการเคลือบผิว นอกจากนี้ จากการทดสอบด้วยเซลล์ไฟฟ้าเคมีทางแสงพบว่า CsPbBr₃/TiO₂ ที่ถูกเคลือบด้วยวิธี in-situ ณ อุณหภูมิ 100 องศาเซลเซียส มีคุณสมบัติถ่ายเทประจุไฟฟ้าที่ดีที่สุด ซึ่งดีกว่าวิธี ex-situ และ CsPbBr₃ QDs ที่ไม่ได้เคลือบด้วย TiO₂

สาขาวิชา วิศวกรรมเคมี

ปีการศึกษา 2563

ลายมือชื่อนิสิต

ลายมือชื่อ อ.ที่ปรึกษาหลัก

ลายมือชื่อ อ.ที่ปรึกษาร่วม

6170208521 : MAJOR CHEMICAL ENGINEERING

KEYWORD: CsPbBr₃ Perovskites, Quantum Dots, Stability, TiO₂

Parina Nuket : Stability Enhancement of CsPbBr₃ Quantum Dots by Coating TiO₂ as a Surface Encapsulation. Advisor: Asst. Prof. Paravee Vas-Umnuy, Ph.D. Co-advisor: Prof. Tetsuya Kida

The cesium lead bromide quantum dots (CsPbBr₃ QDs) have exhibited the excellent optical properties which have been widely used in the applications of optoelectronic and photoelectrochemical devices. However, the instability of CsPbBr₃ QDs against the environment factors has been a major obstacle hindering the commercialization of corresponding devices. Herein, the new encapsulation process, in-situ method, for CsPbBr₃/TiO₂ was presented to prevent the agglomeration of the particles and improve the stability of CsPbBr₃ QDs without heat treatment at high temperature. The CsPbBr₃ QDs were coated with TiO₂ by using titanium tetraisopropoxide (TTIP) as a titanium source which was injected during the formation of CsPbBr₃ QDs in which the effects of TTIP injection temperature from 25°C to 170°C were studied. The morphological, structural, and optical properties of CsPbBr₃/TiO₂ prepared by in-situ method were compared with ex-situ method reported in previous study. Besides preventing an aggregation, the in-situ TiO₂ coated sample at 25°C exhibited the excellent stability against ambient air, non-polar solvent, water and visible light illumination owing to the protection of TiO₂ deposited on the CsPbBr₃ QDs surface and the good structure of CsPbBr₃ QDs. Finally, the photoelectrochemical results showed that the in-situ coated sample at 100°C had the highest charge transport property among the others.

Field of Study: Chemical Engineering

Student's Signature

Academic Year: 2020

Advisor's Signature

Co-advisor's Signature

ACKNOWLEDGEMENTS

First and foremost, I would like to express my deep and since gratitude to my research supervisor, Assistant Professor Paravee Vas-Umnuay, Ph.D., Department of Chemical Engineering, Chulalongkorn University, for giving me the opportunity to do research, providing invaluable guidance and helped me throughout this research.

Moreover, I would also like to thank my co-advisor, Professor Tetsuya Kida, D.Eng., Department of Applied Chemistry and Biochemistry, Kumamoto University, for offering me the research opportunities in his group and leading me working on diverse exciting projects. His dynamism, vision, sincerity and motivation have deeply inspired me. It was a great privilege and honor to work and study under his guidance.

In addition, my sincere thanks goes to Associate Professor Dr. Tawatchai Charinpanitkul, Dr. Rungthiwa Methaapanon and Assistant Professor Weekit Sirisaksoontorn, for their encouragement, insightful comments and participation as the thesis committee.

Finally, my completion of this project could not have been accomplished without the support of my family for their love, caring and total support, as well as the member of KIDA laboratory in Kumamoto University and Center of Excellence in Particle Technology in Chulalongkorn University - thank you for thier friendship, helpfulness and empathy; without them none of this would indeed be possible.

Parina Nuket

TABLE OF CONTENTS

	Page
ABSTRACT (THAI).....	iii
ABSTRACT (ENGLISH).....	iv
ACKNOWLEDGEMENTS.....	v
TABLE OF CONTENTS.....	vi
LIST OF TABLES.....	x
LIST OF FIGURES.....	xi
INTRODUCTION.....	1
1.1 Introduction.....	1
1.2 Objectives of Research.....	3
1.3 Scope of Research.....	3
THEORETICAL BACKGROUND AND LITERATURE REVIEW.....	5
2.1 Perovskite quantum dots (PQDs).....	5
2.1.1 Perovskite compounds.....	5
2.1.2 Quantum dots (QDs).....	6
2.1.3 Applications of PQDs.....	7
2.1.4 Photoelectrochemical (PEC) device of PQDs.....	8
2.1.5 Working principle of perovskite semiconductors.....	9
1) Band Diagram.....	9
2) Bandgap.....	10
2.2 Problems of perovskites stability.....	11
2.2.1 Moisture instability.....	11

2.2.2 Photo-oxidation.....	12
2.2.3 Illumination	12
2.2.4 Thermal instability.....	13
2.3 Strategies of stability enhancement.....	13
2.3.1 Enhancement of moisture stability.....	14
2.3.2 Prevention of photo-oxidation.....	14
2.3.3 Stability enhancement under illumination	15
2.3.4 Enhancement of thermal stability.....	15
2.4 CsPbBr ₃ perovskite quantum dots.....	16
2.4.1 Cesium Lead Bromide (CsPbBr ₃).....	16
2.4.2 Characteristics of CsPbBr ₃ QDs.....	16
2.4.3 Stability of CsPbBr ₃ QDs.....	18
2.5 Titanium dioxide (TiO ₂).....	18
2.5.1 Properties of TiO ₂	18
2.5.2 Applications of amorphous TiO ₂	19
2.6 CsPbBr ₃ QDs coated with TiO ₂	20
2.6.1 Formation mechanisms of TiO ₂	20
2.6.2 Surface encapsulation process of CsPbBr ₃ QDs.....	21
2.7 Literature Reviews.....	22
METHODOLOGY.....	24
3.1 Preparation of CsPbBr ₃ QDs.....	24
3.1.1 Materials.....	24
3.1.2 Synthesis of CsPbBr ₃ QDs	24
3.2 Encapsulation of CsPbBr ₃ QDs with TiO ₂	25

3.2.1 Materials.....	25
3.2.2 Synthesis of CsPbBr ₃ /TiO ₂ by ex-situ method.....	25
3.2.3 Synthesis of CsPbBr ₃ /TiO ₂ by in-situ method.....	25
3.3 Stability testing	26
3.4 Characterization of the samples	27
3.5 Photoelectrochemical characterization.....	27
3.5.1 Cyclic voltammetry (CV).....	27
3.5.2 Current-voltage (IV) characteristics.....	28
CHAPTER 4 RESULTS AND DISCUSSION	29
4.1 Effects of ligand removal processes.....	29
4.2 Morphology and structure of bare CsPbBr ₃ QDs and CsPbBr ₃ /TiO ₂	32
4.2.1 Morphology and particle size distribution.....	32
4.2.2 Elemental and chemical composition	34
4.2.3 Structural properties	35
4.3 Optical properties of bare CsPbBr ₃ QDs and CsPbBr ₃ /TiO ₂	38
4.4 Stability testing	41
4.4.1 Ambient air.....	41
4.4.2 Toluene.....	43
4.4.3 Deionized water with ultrasonication	45
4.4.4 Light illumination	47
4.5 Photoelectrochemical characterizations	49
CHAPTER 5 CONCLUSION	52
5.1 Conclusions	52

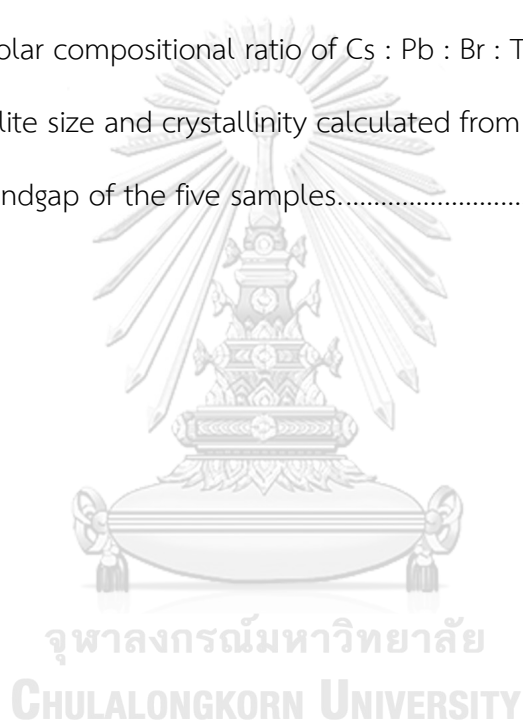
Figure 4.20 48

5.2 Recommendations for the future work.....	53
REFERENCES	54
REFERENCES	58
VITA.....	59



LIST OF TABLES

	Page
Table 1.1 Scope of stability testing.	4
Table 2.1 The general components of perovskite materials.	6
Table 2.2 Properties of TiO ₂ phase. [24].....	19
Table 3.1 Storage conditions of the samples.....	26
Table 4.1 The molar compositional ratio of Cs : Pb : Br : Ti of the five samples.	35
Table 4.2 Crystallite size and crystallinity calculated from XRD results.	37
Table 4.3 The bandgap of the five samples.....	38



LIST OF FIGURES

	Page
Figure 1.1 Scope of synthesis method.	3
Figure 1.2 Scope of characterization.....	4
Figure 2.1 The structure of ABX ₃ perovskite.....	5
Figure 2.2 The comparison of bandgap for bulk semiconductor and quantum dots (left) and the color of light depending on size of quantum dots (right).....	6
Figure 2.3 Applications of PQDs: (a) LEDs, (b) solar cells, (c) PECs, (d) quantum computing, (e) lasers and (f) cell imaging.	7
Figure 2.4 Photoelectrochemical cell with PQDs.....	9
Figure 2.5 Band diagram of electron and hole transportation in photovoltaic devices.....	10
Figure 2.6 Bandgap diagram for conductors, semiconductors, and insulators.....	11
Figure 2.7 UV-Vis absorption and PL emission spectra of CsPbBr ₃ QDs measured by DLS. The excitation wavelength is 365 nm.....	17
Figure 2.8 Orthorhombic, tetragonal, and cubic phases of CsPbBr ₃	17
Figure 2.9 TEM images of CsPbBr ₃ /TiO ₂ (a) before and (b) after annealing at 400°C. 19	19
Figure 2.10 The morphology of TiO ₂ nanocoated particle.....	21
Figure 2.11 In-situ and ex-situ encapsulation process of CsPbBr ₃ /TiO ₂	22
Figure 3.1 Standard three-electrode setup for CV measurement.	28
Figure 3.2 The PEC setup for IV measurement.....	28
Figure 4.1 PL emission spectra of CsPbBr ₃ QDs before and after ligand removal.....	29
Figure 4.2 FT-IR of CsPbBr ₃ QDs before and after centrifugation at different times. .	30
Figure 4.3 Relative FT-IR peak area of ligands at different washing cycles.....	31

Figure 4.4	FT-IR spectra of the samples before and after centrifugation.....	31
Figure 4.5	TEM image and size distribution histogram of bare CsPbBr ₃ QDs synthesized via hot-injection method.	33
Figure 4.6	TEM image and size distribution histogram of CsPbBr ₃ /TiO ₂ coated by in-situ method and injected TTIP at 170°C.	33
Figure 4.7	TEM image and size distribution histogram of CsPbBr ₃ /TiO ₂ coated by in-situ method and injected TTIP at 100°C.	33
Figure 4.8	TEM image and size distribution histogram of CsPbBr ₃ /TiO ₂ coated by in-situ method and injected TTIP at 25°C.	34
Figure 4.9	TEM image of CsPbBr ₃ /TiO ₂ coated by ex-situ method.	34
Figure 4.10	XRD pattern of CsPbBr ₃ QDs and CsPbBr ₃ /TiO ₂ by various methods.	36
Figure 4.11	The relationship between XRD relative intensity of (112) and (110) face to (220) face and the samples synthesized by different methods.....	37
Figure 4.12	The relationship between PLOQ (%) and molar ration of Ti to Cs.	39
Figure 4.13	PL emission spectra and UV-Visible absorption of (a) CsPbBr ₃ QDs, CsPbBr ₃ /TiO ₂ coated by in-situ method (b) at 170°C (c) at 100°C (d) at 25°C and by (e) ex-situ method. The excitation wavelength was 365 nm.	40
Figure 4.14	The comparison of calculated crystallinity for five samples under air.	41
Figure 4.15	Stability of (a) CsPbBr ₃ QDs, CsPbBr ₃ /TiO ₂ coated by in-situ method (b) at 170°C (c) at 100°C (d) at 25°C and by (e) ex-situ method, which were stored under ambient air in powder form.....	42
Figure 4.16	The comparison of relative PL intensity for five samples in toluene.....	43
Figure 4.17	Stability of (a) CsPbBr ₃ QDs, CsPbBr ₃ /TiO ₂ coated by in-situ method (b) at 170°C (c) at 100°C (d) at 25°C and by (e) ex-situ method, which were stored in non-polar solvent (toluene).	44

Figure 4.18 Water stability of (a) CsPbBr ₃ QDs, CsPbBr ₃ /TiO ₂ coated by in-situ method (b) at 170°C (c) at 100°C (d) at 25°C and by (e) ex-situ method, which were ultrasonicated in DIW.	46
Figure 4.19 The comparison of relative PL intensity for the five samples in DIW.....	47
Figure 4.20 Photostability of CsPbBr ₃ QDs, CsPbBr ₃ /TiO ₂ coated by in-situ method at 170°C, 100°C, 25°C and by ex-situ method under light illumination.....	48
Figure 4.21 The comparison of relative PL intensity for the five samples which were dispersed in toluene and continuously soaked visible light source	49
Figure 4.22 The comparison of IV curves for the fives samples in PEC cell (FTO (s) QDs solution, 0.12 M Methanol POM Pt (s))......	50
Figure 4.23 CV curves recorded during the oxidation and reduction of five samples in 0.1 M TBAPF ₆ /Acetonitrile with 10 mV.s ⁻¹ sweep rate (FTO (s) QDs solution Pt (s))......	51

CHAPTER 1

INTRODUCTION

1.1 Introduction

Perovskite is one of the most promising semiconductor materials which has a structure of ABX_3 , where A is methylammonium (MA) or formamidinium (FA); B is lead or tin; and X is halides. The perovskite materials have been studied extensively owing to their good optical properties which were widely used in the applications of optoelectronic devices [1]. However, the instability of the perovskite materials has still been a problem which is affected by extrinsic factors including moisture and oxygen, and also by intrinsic factors including hygroscopicity, thermal instability and ion migration. The all-inorganic cesium lead bromide ($CsPbBr_3$) perovskites with the nanocrystal size or quantum dots (QDs) have been reported with the excellent stability compared to other types of perovskite as well as a greater confinement energy and the tunable bandgap. Nevertheless, the stability of perovskite quantum dots (PQDs) is still limited for optoelectronic and photoelectrochemical applications because PQDs can be decomposed by water and oxygen attacking. In order to prevent the decomposition of QDs, the surface encapsulation is focused in this work.

Previously, Z. Li et al. synthesized $CsPbBr_3$ QDs encapsulated with TiO_2 by adding titanium butoxide (TBOT) as a titanium precursor. TiO_2 shell coating diminished anion exchange and photodegradation, resulting in the enhancement of stability for more than 3 months [2]. Besides the stability improvement, A. D. Pramata et al. has used the TiO_2 coating technique for $CsPbBr_xI_{3-x}$ QDs to control the PL emission by transferring the excited electron to polyoxometalates (POM). The results showed that TiO_2 can allow the charge transportation in the particle, which was an interesting advantage for coating perovskite QDs with TiO_2 . However, the encapsulation method in previous studies still caused the agglomeration of QDs within TiO_2 shell because the ligands preventing the agglomeration of QDs were removed before encapsulation process. The agglomeration of QDs would generate a trap sites and cause loss of their efficiency in some important applications. Sievers et

al. has reported a new method to prepare polypropylene/TiO₂ through the in-situ synthesis of nanostructured TiO₂ that directly added titanium precursor in the polymer solution, which can avoid the agglomeration during the step of mixing the TiO₂ and PP [3]. Similarly, Cao et al. has presented the single-step synthesis of CsPbBr₃/SiO₂ core/shell, in which each core/shell had only one CsPbBr₃ QDs [4].

Herein, the CsPbBr₃ QDs were synthesized via hot injection with three-precursor approach techniques, modified by M. Imran et al., in order to obtain a higher quality of QDs and a higher level of particle-size control [5]. Then, the CsPbBr₃ QDs were coated with TiO₂ via the in-situ method compared to the previous process, ex-situ method. Titanium tetraisopropoxide (TTIP) was used as the titanium source. Moreover, the effects of TTIP injection temperature from 25°C to 170°C in the in-situ method were studied since the titanium precursor possibly disrupted the reaction for perovskite formation. To investigate the stability enhancement of CsPbBr₃ QDs and CsPbBr₃/TiO₂, the storage conditions were tested in the following conditions: 1) under ambient air 2) in toluene, 3) in deionized water with ultrasonication, and 4) under continuous soaking light. The crystallinity and PL intensity of the samples were monitored to observe the change in their stability at different times. In addition, the morphological, structural and optical properties of CsPbBr₃ QDs/TiO₂ have been studied to understand the effects of surface encapsulation method. Finally, the photoelectrochemical cell was used to characterize the charge transport properties of CsPbBr₃/TiO₂ synthesized via in-situ and ex-situ methods.

1.2 Objectives of Research

1. To study the effects of in-situ and ex-situ encapsulation methods on the morphological, structural and optical properties of CsPbBr₃/TiO₂.
2. To investigate and compare the stability of bare CsPbBr₃ QD and CsPbBr₃/TiO₂ at various conditions including under ambient air, in toluene, in deionized water and under light illumination.
3. To investigate the charge transport properties of CsPbBr₃/TiO₂ compared to CsPbBr₃ QDs by using photoelectrochemical characterization.

1.3 Scope of Research

The scopes of this research were divided into 3 parts as follows: 1) scope of synthesis method, 2) scope of stability testing and 3) scope of characterizations.

For the synthesis method, the CsPbBr₃ QDs were synthesized via hot-injection method improved from M. Imran et al. and were coated by ex-situ and in-situ method using TTIP as titanium precursor to compare the stability and properties of the sample encapsulated by various processes (figure 1.1).

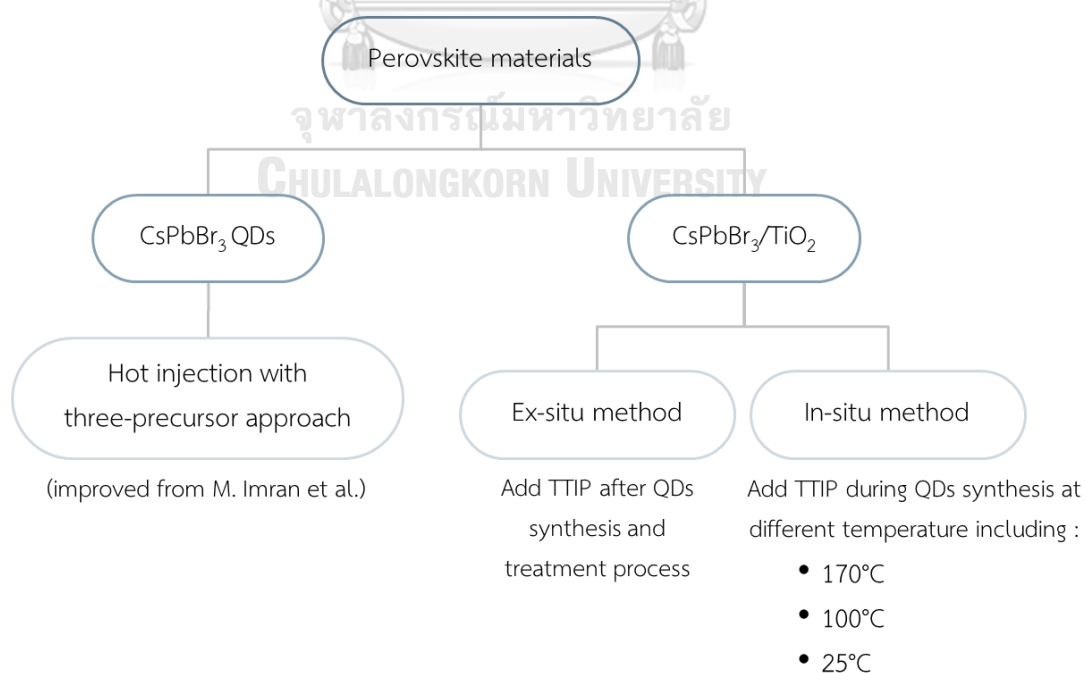


Figure 1.1 Scope of synthesis method.

For the stability testing, the bare CsPbBr₃ QDs and CsPbBr₃/TiO₂ coated by ex-situ and in-situ methods were kept under various conditions, including 1) under ambient air, 2) in toluene, 3) in deionized water, and 4) under continuous soaking light. The stability of the samples was investigated from the crystallinity calculated from XRD results and the PL emission at different time (table 1.1).

Table 1.1 Scope of stability testing.

Testing conditions	Media	Time range	Characterization
1) Ambient air (70%RH, 28°C)	Powder form	5 days	Crystallinity
2) Non-polar solvent (25°C)	Toluene	7 days	PL intensity
3) Water with ultrasonication	Deionized water	30 min	PL intensity
4) Visible light illumination	Toluene	80 min	PL intensity

For the effects of coating TiO₂ on CsPbBr₃ QDs, the morphological, structural and optical properties were investigated by TEM, FT-IR, XRF, XRD, UV-Visible spectrophotometer and PL spectrometer. In addition, the charge transport properties of the samples were characterized by using photoelectrochemical cell (figure 1.2).

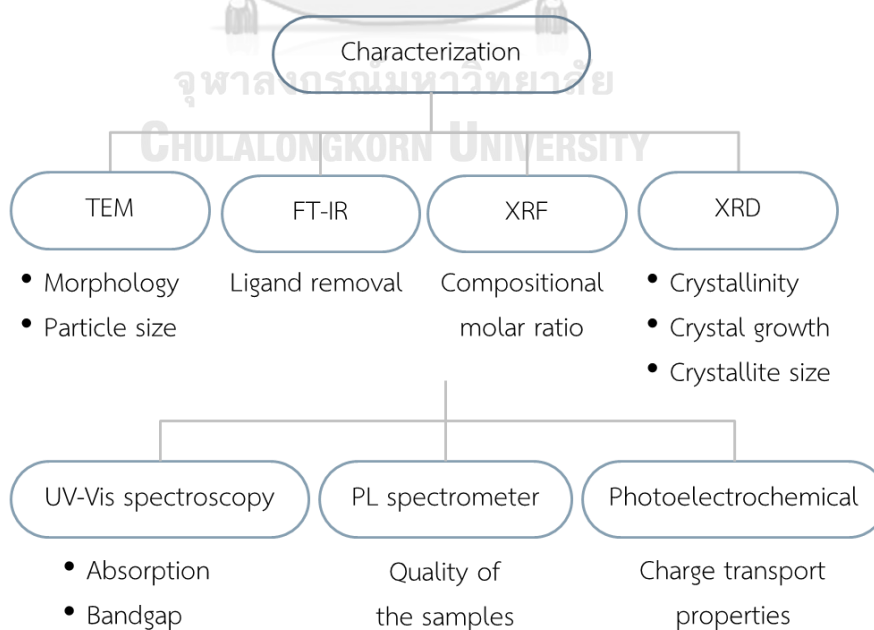


Figure 1.2 Scope of characterization.

CHAPTER 2

THEORETICAL BACKGROUND AND LITERATURE REVIEW

2.1 Perovskite quantum dots (PQDs)

Perovskite quantum dots are semiconducting nanocrystals. Compared to metal chalcogenide quantum dots, perovskite quantum dots are more tolerant to defects and have excellent photoluminescence quantum yields and high color purity. These properties are highly desirable for electronic and optoelectronic applications and hence perovskite quantum dots have huge potential for real world applications including LED displays and quantum dot solar cells.

2.1.1 Perovskite compounds

A perovskite is a name of mineral, CaTiO_3 , that was found in the Ural Mountains by Lev Perovski. Meanwhile, a perovskite is generally called for any compound that has the same type of crystal structure as the perovskite mineral, ABX_3 , where A is a cation at the corner of the lattice, B is another type of cation at the center of the lattice and X is an anion occupied at the face of the lattice (figure 2.1). In general, A is an organic cation or an inorganic cation, B is a cation of lead (II) and X is a slightly smaller halogen anion. [6]

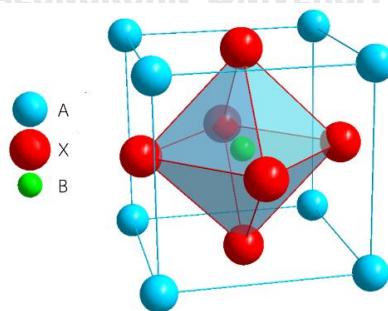


Figure 2.1 The structure of ABX_3 perovskite.

The type of atoms or molecules used in the ABX_3 structure affects their properties. The different structures lead to the different properties such as conductivity, optical and catalytic properties. The perovskite materials can be divided

into 2 categories: hybrid organic-inorganic perovskite (HOIP) and all-inorganic perovskite (AIP), depending on the type of cation A, as shown in table 2.1 [7].

Table 2.1 The general components of perovskite materials.

Types of Perovskite	A	B	X ₃
HOIP	Methylammonium (CH ₃ NH ₃ ⁺), Formamidinium (NH ₂ CHNH ₂ ⁺)	Lead (Pb ²⁺), Tin (Sn ²⁺)	Chloride (Cl ⁻), Bromide (Br ⁻), Iodide (I ⁻)
AIP	Cesium (Cs ⁺)		

2.1.2 Quantum dots (QDs)

Quantum Dots (QDs) are nanoscale crystals with diameters in the range of 2-10 nm, and exhibit the excellent optical properties including narrow emission widths, high quantum yields and tunable band gaps with over the IR-UV range via controlling their size, halide substitution and quantum confinement effects. Generally, as the size of the crystal decreases, the difference in energy (bandgap) between the highest valence band and the lowest conduction band increases. More energy is then needed to excite the dot, and concurrently, more energy is released when the crystal returns to its ground state, resulting in a color shift from red to blue in the emitted light as shown in figure 2.2.

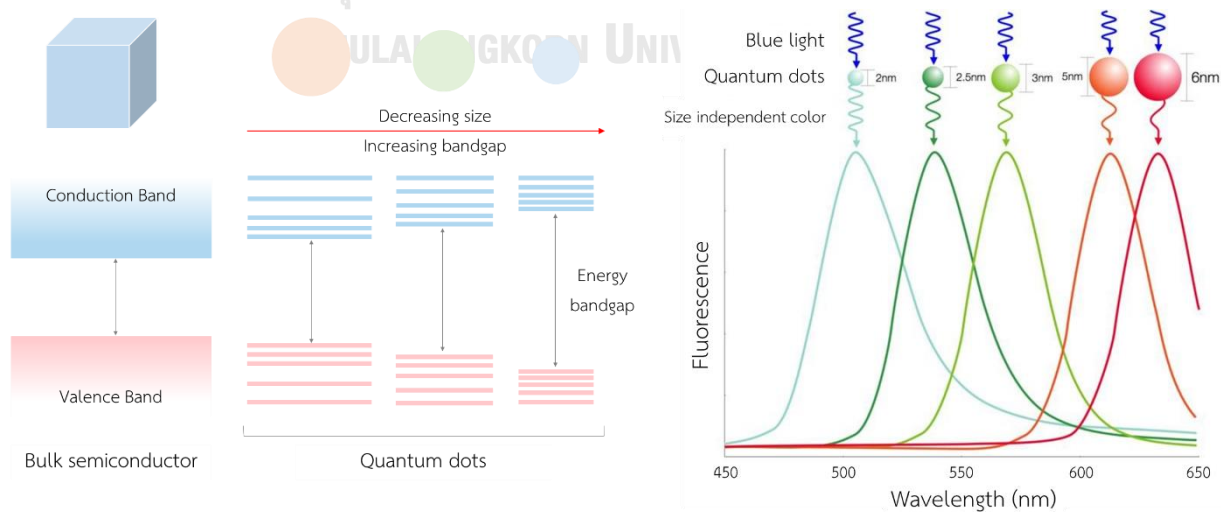


Figure 2.2 The comparison of bandgap for bulk semiconductor and quantum dots (left) and the color of light depending on size of quantum dots (right).

Besides the optical properties, decreasing the particle size to QDs also improves the stability of materials, for example, CsPbI₃ QDs can be synthesized at room temperature, while the bulk cubic of CsPbI₃ perovskite cannot be stable at temperature less than 328°C. Ruo Xi Yang and Liang Z. Tan has used density function theory to describe the size dependence of phase stability in perovskite nanocrystals. The optically active phases (α - and γ -phase) were found to be thermodynamically stabilized against the yellow δ -phase by reducing the size of the nanocrystal due to the smaller total energy of these phases than yellow δ -phase.

2.1.3 Applications of PQDs

The unique size and composition tunable electronic property of the semiconducting quantum dots make them very appealing for a variety of applications and new technologies. In addition, the advantages of using PQDs for making the devices are as followed: (1) they can be synthesized under room temperature, (2) they can be made from an inexpensive material without extensive purification, as silicon does, and (3) they can be applied to a cheap and flexible substrate materials. Potential applications for PQDs include light emitting diodes (LEDs), solar cells, photoelectrochemical (PEC), lasers, photodetectors, quantum computing, cell imaging and cancer mapping as shown in figure 2.3.

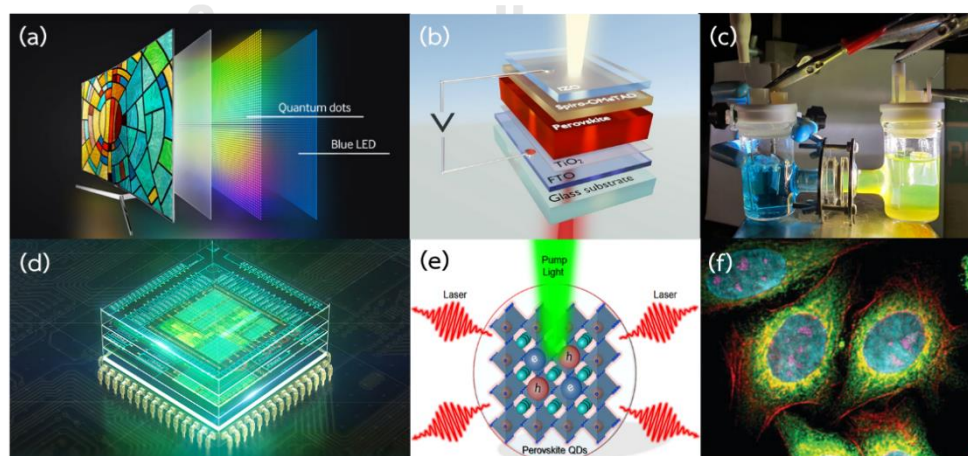


Figure 2.3 Applications of PQDs: (a) LEDs, (b) solar cells, (c) PECs, (d) quantum computing, (e) lasers and (f) cell imaging.

Most of applications as mentioned above are called optoelectronic devices which are electrical-to-optical or optical-to-electrical transducers. The light relating to the devices includes invisible forms of radiation such as gamma rays, X-rays, ultraviolet and infrared, in addition to visible light. However, the devices focused in this work are the photoelectrochemical device using visible light as an energy source which is explained in the next section.

2.1.4 Photoelectrochemical (PEC) device of PQDs

The photoelectrochemical (PEC) device works either in photo-catalyst mode where the electrochemical reaction is occurred by light inducing and could produce the useful products, or designed in photovoltaic mode such as dye-sensitized solar cell where the cell generates the electrical power. The PEC device is fundamentally about the light absorption, charge creation and their separation which works on the photon energy conversion. Moreover, the processes involve the interfaces between semiconductor and electrolyte, which is different from the solar cells involving the interfaces between semiconductor and metal [8]. In the case of PQDs, the PQDs can create highly energetic electrons and holes through the absorption of visible light. These electrons and holes can drive the conversion of some reactants into high value products which is called the direct conversion of light into chemical energy.

For the system in this work, the PQDs were used as a charge generator by visible light absorption as shown in figure 2.4. After generation of electrons and holes, electrons were transferred to the working electrode (FTO) and counter electrode (Pt mesh). Then, polyoxometalate (POM) in electrolyte accepted the electrons at the cathode site and was reduced to POM^- while holes in valence band maximum of PQDs were accepted by methanol which was able to be oxidized to formaldehyde or combusted to CO_2 . The benefit of PEC was we can investigate the charge transfer of PQDs from the current–voltage (I–V) relations deriving from the charge transfer reactions between PQDs in electrolyte and electrode interfaces. The higher charge transfer property facilitated the higher current of PEC system. [9, 10]

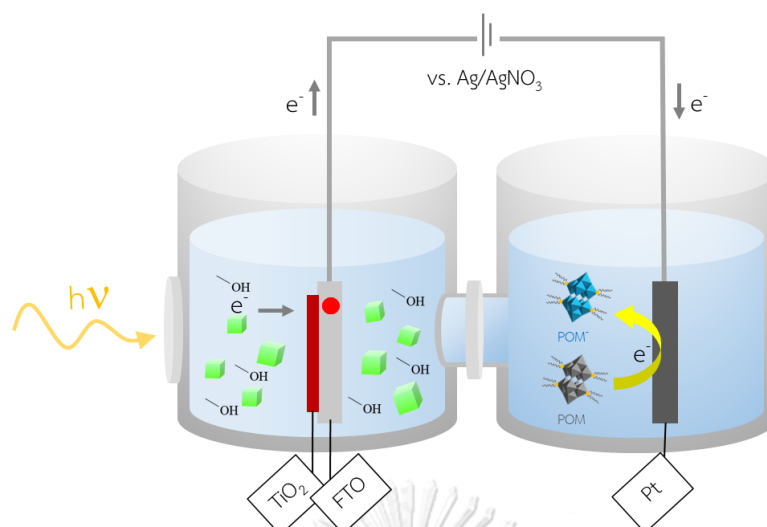


Figure 2.4 Photoelectrochemical cell with PQDs.

2.1.5 Working principle of perovskite semiconductors

In terms of working principle, when solar energy is absorbed by perovskite layer and a valence electron of perovskite gains enough energy, the valence electron can escape from the HOMO (highest occupied molecular orbital level) of valence band to the LUMO (lowest unoccupied molecular orbital) of conduction band, while the vacancy or hole is left in the HOMO. This process is called “charge separation”. Electrons and holes will be transferred through the LUMO of ETL (electron transport layer) to cathode, and the HOMO of HTL (hole transport layer) to anode, respectively, by charge-selective contacts. This chain reaction of hole and electron movement will create current in the system.

1) Band Diagram

The key factor of this device operation is the energy level or band diagram of each material in the device (figure 2.5). For example, in photovoltaic device, the energy levels of each material in the device have to match with the valence band and conduction band of perovskite because an equilibrium conditions can be reached in which a voltage difference leading to transferring of charges. Conduction band of ETL must lie under conduction band of the active perovskite layer to extract

electrons from the excitons arriving the interface. Its valence band must be lower than the valence band of perovskite to reject the holes from entering this layer. Similar conditions hold for the HTL. The valence band of HTL must lie above the valence band of perovskite to attract the holes from perovskite layer and prevent transferring of the electron in HTL. [11]

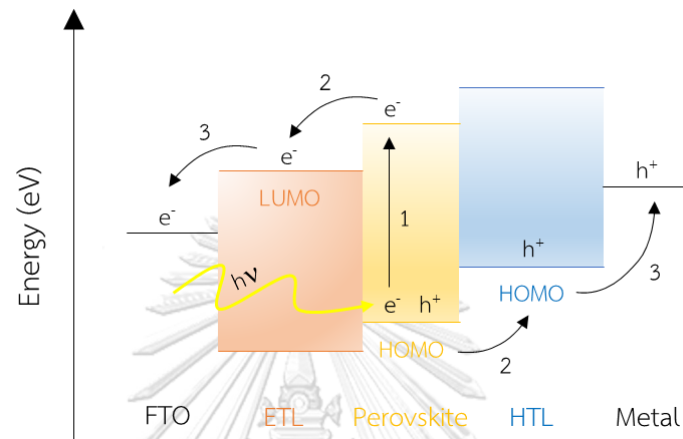


Figure 2.5 Band diagram of electron and hole transportation in photovoltaic devices.

2) Bandgap

Besides the band diagram, in order to transfer electrons to the conduction band, the amount of energy that they receive from external source such as sun must be more than the different amount of energy between valence band and conduction band, which is called “bandgap”. The bandgap initiates a different conductivity of materials which can be divided into 3 types of material: insulator, semiconductor and conductor. From the energy diagram of these materials (figure 2.6), an insulator has the biggest band gap. The electrons cannot jump to the conduction band that is why it does not conduct current. The band gap in a semiconductor is smaller than an insulator and allows valence electrons to jump to the conduction band if it receives external energy as happened in perovskite. In a conductor, i.e., copper, the conduction band and valence band overlap thus there is no bandgap, which means that electrons can freely move into the conduction band as a sea of electrons. It is used as a cathode and an anode in the electronic devices. [11]

The ideal band gap for photovoltaic devices has to be counterbalanced because a low band gap is desired to absorb as much of the solar spectrum as possible, while a larger band gap affects a large built-in voltage. Due to a range of 0.5 eV to 3.2 eV of entire sunlight spectrum, the ideal band gap should be between 1.0 and 1.7 eV to motivate electrons without creating too much heat. [12]

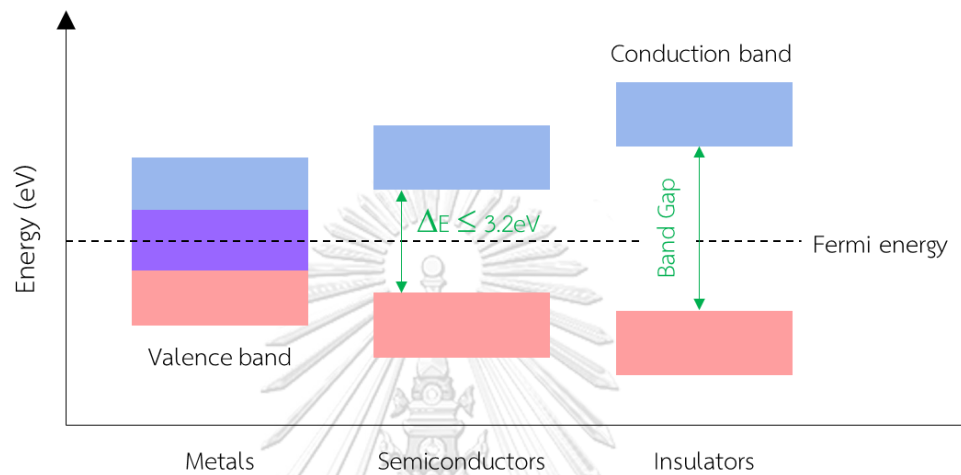


Figure 2.6 Bandgap diagram for conductors, semiconductors, and insulators.

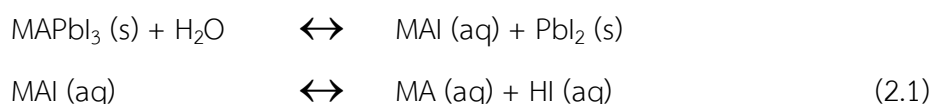
2.2 Problems of perovskites stability

Although various HOIPs, e.g., MAPbI_3 , have been greatly studied as the light absorber in optoelectronic devices because of the good optical properties, the main problem of HOIPs is their low stability under ambient atmosphere. This is because hydrogen bond between organic cation and lead halide of HOIP is very weak, so that it can degrade PbI_2 easily in common conditions including moisture, photo-oxidation by oxygen, illumination and thermal instability.

2.2.1 Moisture instability

Although the devices are packaged tightly, there is a probability of leakage. Moreover, the devices have to be operated and transported through air in the factory before packaging. Therefore, the perovskite material should exhibit high moisture stability. The water molecules can penetrate the perovskite structure and form an intermediate monohydrate and dihydrate perovskite. The strong hydrogen

bonds between water molecules and organic cations are formed in perovskite crystal while the bonds between organic cations and PbI_3 are very weak. Thus, it leads to a faster deprotonation of the organic cation. After perovskite degradation, water molecules protonate iodide which create volatile hydroiodic acid (HI), and yellow lead iodide (PbI_2) are left as shown in the reaction of decomposition [13, 14].



2.2.2 Photo-oxidation

As described previously, oxygen is one of among important factors affecting the perovskite stability and packaging is not the best way to prevent contacting with oxygen because of high cost and potential failures. Metal halide perovskites are stable to oxygen when left in the dark. However, A. J. Pearson et al. found that MAPbI_3 absorber degraded by 20% within a few hours of 1 sun exposure in the presence of both oxygen and light and the degradation rate increased following higher amount of oxygen [15]. Haque et al. explained that oxygen was adsorbed and diffused in perovskite lattice through iodide vacancies, which was generated by photoexcitation, because these iodide vacancies have a similar volume with oxygen molecule. The oxygen molecule will trap electrons in the conduction band of photoexcited perovskite to form highly reactive superoxide O_2^- , which react with the acidic A-site cation and create A-site gas, water and lead iodide [13].

2.2.3 Illumination

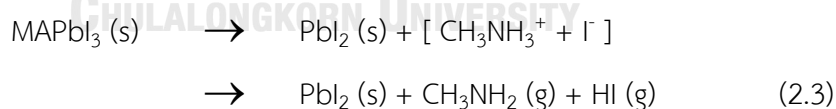
The illumination can affect the degradation of perovskite, even though in the absence of other environment factors such as oxygen. There are reports that there are significant effects in perovskite film during illumination, including ion migration, halide segregation, and compositional degradation. DeQuilettes et al. showed that there is a migration of I^- species away from the illuminated area in MAPbI_3 films after testing under 1 sun equivalent irradiation intensity [13, 16].

2.2.4 Thermal instability

Temperature is another important parameter affecting phase of perovskite directly. Its compound should remain in the desired photoactive structure during processing without transforming to a non-photoactive phase. The structure stability of ABX_3 can calculate in terms of Goldschmidt tolerance factor, t :

$$t = \frac{r_A + r_B}{\sqrt{2}(r_B + r_X)} \quad (2.2)$$

where r is the radius for A cation, B cation and X anion, and perovskite structures are formed when t is between 0.71 and 1. This equation suggests that formamidinium (FA) cation is too large and cesium (Cs) cation is too small for perovskite structure so that they tend to revert to a non-photoactive and yellow delta phase at room temperature. While methylammonium (MA) cation has a tolerance factor of 0.91 and can maintain a photoactive phase, black tetragonal or cubic phase, under operational temperature from -15 to 65°C [13]. However, MA perovskites as organic compounds have a less resistance of thermal decomposition due to a higher volatility compared to inorganic salts. Kim et al. heated MAPbI_3 films at 80°C for 1 h and found that the structure changed to an intermediate phase and followed by escape of CH_3I and NH_3 :



2.3 Strategies of stability enhancement

As discussed above, the degradation factors of perovskite can be diminished by many methods such as improving the perovskite structure through its components or adding a dopant, modifying its top surface and grain, passivating its surface to prevent penetrating of some species into its structure and decreasing the crystal size to nanoscale. These strategies are discussed following its stability issues.

2.3.1 Enhancement of moisture stability

X-site halide substitution can shrink the perovskite lattice and stabilize the cubic perovskite. For example, Noh et al. reported that substituting iodide with smaller bromide at 20-29% of Br, $\text{MAPb}(\text{I}_{1-x}\text{Br}_x)_3$ resulted in a better performance and higher stability because of the stronger interaction between organic cation and lead halide. Moreover, mixing Cs in FAPbI_3 can enhance the moisture stability under normal humidity to 90%RH [17].

A-site cation substitution such as CsPbBr_3 can keep in 60-70%RH over 15 days with small degradation, while performance of MAPbBr_3 cells dropped by 80% [18]. However, X-site halide anion is also important. When substituting Br^- by I^- , it was reported that CsPbI_3 was less stable under high humidity and it reverted from black cubic to yellow orthorhombic phase.

The simpler ways are modifying the film surface and controlling grain boundaries to minimize the degradation from moisture. Large grains have fewer defects which usually lie at the grain boundaries and also longer nonradiative lifetimes and larger diffusion length resulting in high performance of photovoltaic devices. Besides improving the perovskite material, the charge transport layer and top electrode can be made from non-corrosive and hydrophobic material to protect the perovskite from moisture such as carbon and metal oxide-based electrodes [13].

2.3.2 Prevention of photo-oxidation

Due to the iodide vacancies in perovskite structure offering a facile path for oxygen, controlling the density of iodide vacancies is the solution. Saidaminov et al. added smaller cadmium cations as a B-site dopant to the perovskite which suppress vacancy formation and resulted in an increase of stability under ambient air [19].

In addition, the degradation mechanism involves an acid-base reaction of highly reactive superoxide O_2^- and acidic A-site cation. Thus, less acidic cations such as FA and Cs can hinder this pathway and be stable to photo-oxidation [13].

B-site metal also affects the oxidation toleration. For instance, tin(II)-based perovskite is less stable to oxygen compared to lead and can oxidize even in the dark because tin(II) is very sensible to oxidation to tin(IV) as followed:



As a result, B-site should be occupied by the elements that only exist in the (II) oxidation state such as lead(II).

2.3.3 Stability enhancement under illumination

Passivation can hinder the ionic species to diffuse throughout the perovskite structure because there is the migration of I^- species occurred after illumination. Moreover, the stronger bond between cation and halide anion is necessary for binding. Moreover, superoxide molecules passivation was desired, where oxygen can be adsorbed to surface-trapped electrons and form a stable superoxide-defect complex that moves the defect energy level outside of the band gap. [13]

2.3.4 Enhancement of thermal stability

Since organic compounds have a less resistance of thermal decomposition compared to inorganic compounds, all-inorganic perovskites have been considered as a durable material. Among all-inorganic perovskite materials, $CsPbX_3$ is the most appropriate candidate due to its high valence band position (VBP) and high thermal stability. However, X-site halogen has a significant influence for thermal tolerance and has proven to improve structure stability by substituting I^- with Br^- because the $CsPbI_3$ cubic perovskite phase is not stable at room temperature (less than 328°C) and transforms to yellow non-perovskite phase spontaneously in a matter of minutes [20], while $CsPbBr_3$ has two phase transitions, cubic-tetragonal (130°C) and orthorhombic (88 °C), with hardly any color change [21]. In addition, limiting crystal size in nanoscale can form more stable phase at room temperature. The nano-sized perovskite will be discussed in the next section.

2.4 CsPbBr₃ perovskite quantum dots

To understand the important of CsPbBr₃ QDs, especially in optoelectronic applications, it will be focused in terms of its advantages, characteristics and stability of CsPbBr₃ QDs.

2.4.1 Cesium Lead Bromide (CsPbBr₃)

There are many ways to improve the stability as described previously but the most interesting way is the substitution of organic cations by inorganic cations, Cs, as all-inorganic perovskites because Cs cation has proven that :

- (1) In terms of moisture, CsPbBr₃ can keep in 60-70%RH over 15 days with small degradation that is more stable than hybrid perovskite.
- (2) In terms of oxidation, Cs is less acidic cation that can hinder degradation mechanism of acid-base reaction and be stable to photo-oxidation.
- (3) In terms of illumination, the bond between Cs cation and lead halide is stronger than organic cation so it might prevent the migration of I⁻ occurred after illumination.
- (4) In terms of heat, it appears that inorganic compounds have a higher resistance of thermal decomposition due to a less volatility.

In addition, when compared the X-site halogen anion of CsPbX₃ between I⁻ and Br⁻, CsPbBr₃ is more stable because of the lower phase transition temperature, while CsPbI₃ turns into yellow phase spontaneously at room temperature.

2.4.2 Characteristics of CsPbBr₃ QDs

CsPbBr₃ QDs were generally synthesized by using hot injection method. They exhibited high photoluminescence (PL) performance with PLQY of green emission as high as 90% and PL peak of 515 nm (figure 2.7). The phase stability of CsPbBr₃ QDs is divided into 3 phases according to the temperatures that are cubic α -phase (>130°C), tetragonal β -phase (88-130°C) and orthorhombic γ -phase (<88°C) [22] (figure 2.8).

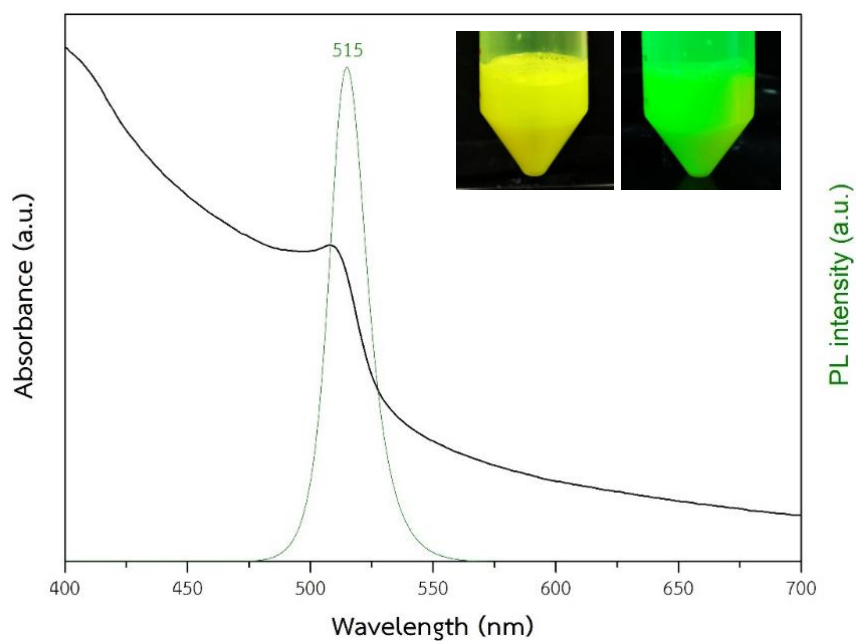


Figure 2.7 UV-Vis absorption and PL emission spectra of CsPbBr₃ QDs measured by DLS. The excitation wavelength is 365 nm.

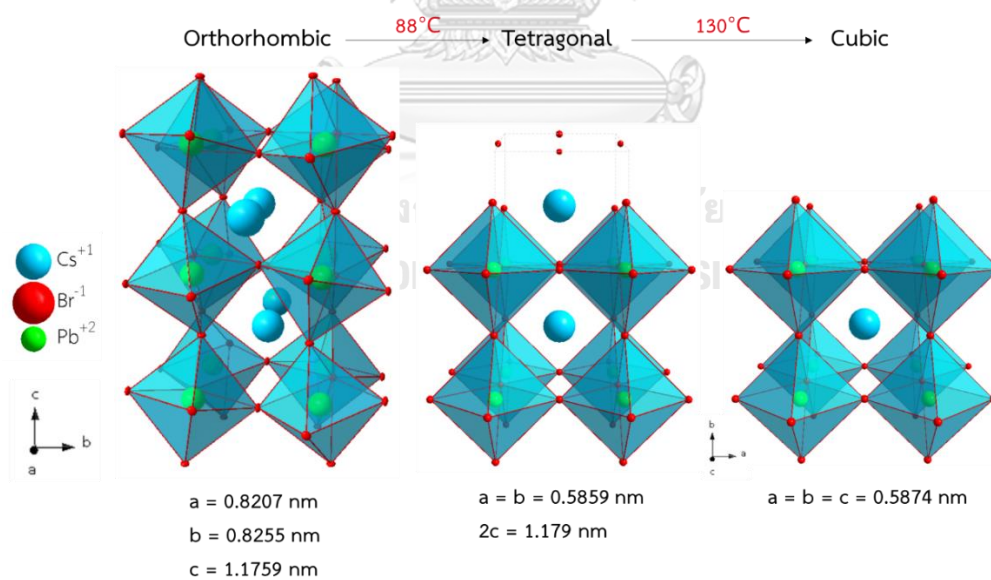


Figure 2.8 Orthorhombic, tetragonal, and cubic phases of CsPbBr₃.

2.4.3 Stability of CsPbBr₃ QDs

Although the overall stability of CsPbBr₃ QDs is better than hybrid organic-inorganic, CsPbBr₃ QDs still suffer from losing their structure because of the presence of water via hydration (or solvation in other polar solvents) so they have to be stored in non-aqueous media such as toluene. However, for optoelectronic applications, CsPbBr₃ QDs are usually deposited on the substrate without any media so the moist environment can degrade the perovskite structure easily. In addition, mixing different halide perovskite QDs can lead to fast anion-exchange with a composition homogenization [2]. Therefore, there is an attempt preventing the moisture by surface modification with water-proof capping ligands, encapsulation using polymer matrices and surface coating. Most of all, the selected strategy must not restrict the charge transport for solar cell application.

2.5 Titanium dioxide (TiO₂)

Titanium dioxide (TiO₂) is an important oxide material in a solid state chemistry. It has been used in numerous commercial applications such as an opacifying agent in paints, plastics, corrosion-resistance coatings and etc. Especially, it has been extensively studied for applications in electronic devices because of its electronic structure. Optoelectronic device is one of the applications that generally uses TiO₂ as a charge transport layer and the stability enhancement material.

2.5.1 Properties of TiO₂

TiO₂ is a simple inorganic compound which is widely used as the charge transport material because the suitable energy level of HOMO and LUMO in valence band and conduction band so it can transfer electrons and hinder holes. The common forms of TiO₂ applied in various applications are amorphous phase (non-crystalline) and crystalline phase of anatase and rutile. The properties of TiO₂ are shown in table 2.2. The bandgap of TiO₂ is in the range of 3.00-3.50 eV that can absorb UV light (350 - 410 nm) and offers good transmission between 400 and 700

nm by tuning the intrinsic refractive index, the size of the particles and their film thickness. [23] Furthermore, it has high resistance towards acid and alkali and non-poisonous, so it has been used in various applications.

Table 2.2 Properties of TiO₂ phase. [24]

TiO ₂ phase	Mass density (g.cm ⁻³)	Bandgap (eV)
Amorphous	3.85	3.42
Anatase	4.07	3.02
Rutile	3.79	3.35

However, to transform the amorphous phase to the crystalline phase of TiO₂, the high annealing temperature is required but the PQDs is very sensitive to the heat. The heat treatment leads to grain growth of perovskite material and increase of the particle size, which would lose the properties of quantum dots (figure 2.9).

(a) Before annealing

(b) After annealing

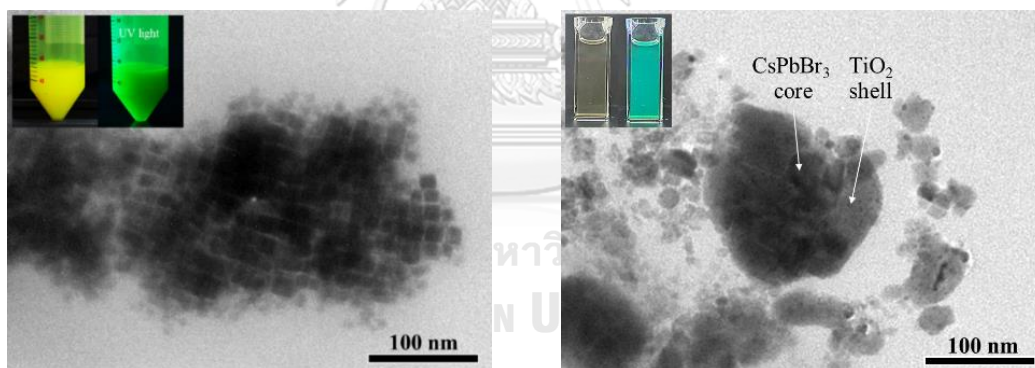


Figure 2.9 TEM images of CsPbBr₃/TiO₂ (a) before and (b) after annealing at 400°C.

2.5.2 Applications of amorphous TiO₂

Due to the thermal instability of CsPbBr₃ QDs, amorphous TiO₂ was considered in this work. Amorphous TiO₂ has been reported in water splitting application by Lee et al. that a thin layer of amorphous TiO₂ on CdSe QDs showed a highly efficient charge separation which allowed the electrons in the conduction band of CdSe to migrate to that of amorphous TiO₂ in which the electrons were

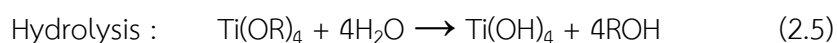
participated in hydrogen production, while the holes remaining in the valence band of CdSe QDs was scavenged by Na₂S and Na₂SO₃. Therefore, the introduction of amorphous TiO₂ nanoshells can hinder charge recombination, facilitate charge separation and reduce charge transfer resistance, finally leading to significantly enhanced photocatalytic performance [25]. Moreover, it has been found that O–O peroxy linkages were generated in pristine amorphous TiO₂ upon injection of excess holes, and gave a defect distribution centered above the valence band, leading to hole diffusion in amorphous TiO₂ through an exchange mechanism [24]. Consequently, the amorphous TiO₂ did not only protect the photocatalyst from degradation, but it also allowed the photogenerated holes to diffuse through the amorphous and to reach the interface with electrolyte, thus behaving as a leaky channel rather than as an insulating layer, which was very useful in PEC devices.

2.6 CsPbBr₃ QDs coated with TiO₂

Recently, there are many studies that try to improve the stability of PQDs by surface modification of PQDs with water-proof capping ligands and encapsulation with polymer matrices or SiO₂, etc. Although the stability of PQDs has been enhanced by previous method, these polymers and SiO₂ shell prevented the charge transport for the optoelectronic and PEC applications. Therefore, the TiO₂ was used to passivate the CsPbBr₃ QDs due to the high chemical stability and the electrical conductivity of the TiO₂ shell. In this section, the formation mechanisms of TiO₂ during the encapsulation process of in-situ and ex-situ method are presented.

2.6.1 Formation mechanisms of TiO₂

The sol-gel method is used for TiO₂ synthesis through the hydrolysis and condensation of titanium alkoxides (Ti(OR)_n) in aqueous media, where R is i-propyl. The reactions are shown as follows.



Alkoxide is hydrolyzed when there is a presence of water and subsequently polymerized to form a three-dimensional oxide network. It is well known that the tetravalent cations are too acidic so that the nucleation of stable hydroxide $\text{Ti}(\text{OH})_4$ cannot occur. Then it leads to an amorphous oxide of TiO_2 which is gradually adsorbed and deposited on the surface of CsPbBr_3 QDs [2]. The morphology of coated nanoparticles is shown in figure 2.10.

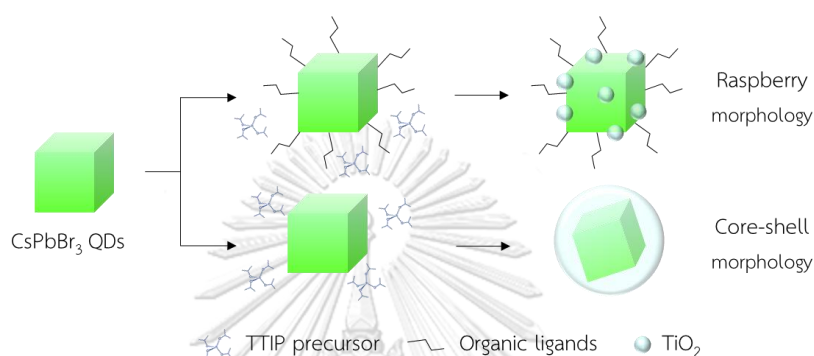


Figure 2.10 The morphology of TiO_2 nanocoated particle.

2.6.2 Surface encapsulation process of CsPbBr_3 QDs

Surface encapsulation process can be divided into 2 types (figure 2.11) including (1) ex-situ synthesis (multiple steps) where the core material is formed first, followed by ligand removal and suspending in the solvents, then a coating is done, (2) in-situ synthesis (single step) where the coating is done at the same time as core particle is formed, then the particles are treated by removing the ligands to enhance the charge transfer of CsPbBr_3 QDs. Although both processes are derived by the sol-gel synthesis, the different morphology could be obtained by changing the step of titanium precursor injection. Generally, the core-shell morphology is better controlled via sol-gel method as seen in the ex-situ method. However, the ligands surrounding the CsPbBr_3 QDs could affect the deposition of TiO_2 on QDs surface. Instead of core-shell morphology, the raspberry morphology could be obtained due to the ligand-restricted adsorption of TiO_2 as seen in the in-situ method.

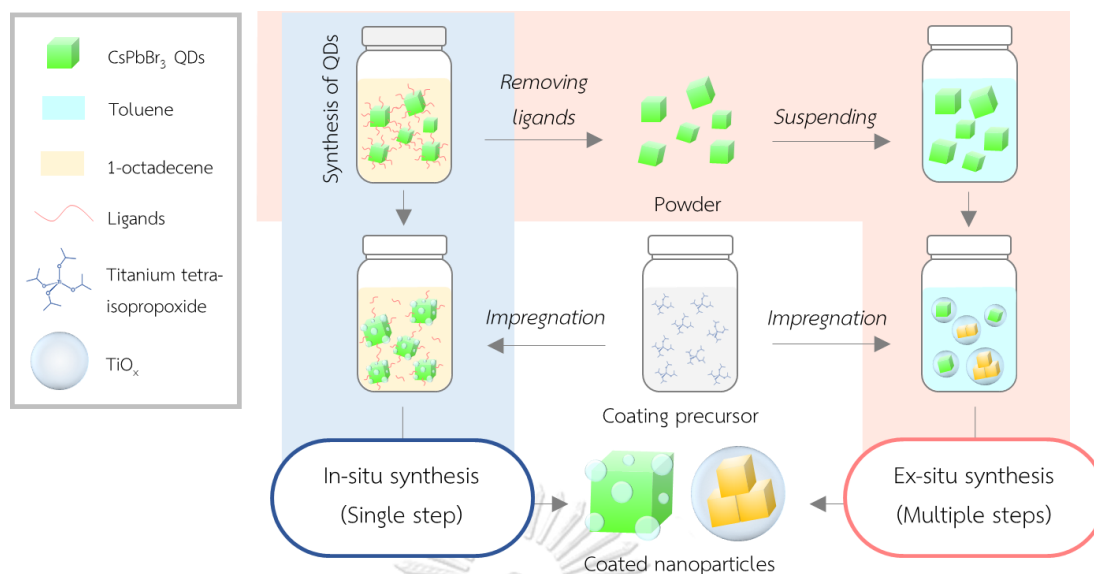


Figure 2.11 In-situ and ex-situ encapsulation process of CsPbBr₃/TiO₂.

2.7 Literature Reviews

Z. Zheng et al. shielded the SiO₂ around CsPbI₃ QDs that were prepared through the hot-injection method with average size of 15 nm. (3-aminopropyl)triethoxysilane (APTES) was used as the SiO₂-capping agent to address low PL stability of moisture, oxygen and heat. After soaking the SiO₂-coated CsPbI₃ QDs in a boiling water for 48 h, the QDs can keep 95% of their initial PL intensity, while the bare CsPbI₃ QDs can keep only 30% of their initial PL intensity. This CsPbI₃/SiO₂ core/shell nanocrystals not only kept the fluorescent color, but also improved moisture-, oxygen-, and thermal PL quenching due to shielding of SiO₂ layer against air and water around CsPbI₃ QDs. [26]

According to previous studies, coating CsPbBr₃ QDs with another material on a single-particle level was very difficult. Cao et al. presented the single-step synthesis of CsPbBr₃/SiO₂ core/shell, in which each core/shell had only one CsPbBr₃ QDs. The results suggested that the ligands of oleic acid and oleylamine had an important role for the formation of uniform SiO₂ shell on the CsPbBr₃ surface and preventing the aggregation between CsPbBr₃ QDs during single-step synthesis. Besides monodisperse CsPbBr₃/SiO₂ core-shell QDs, SiO₂ core shell can prevent the damage of water and the PL emission was maintained above 100% after the ultrasonication in deionized

water for 40 min. Moreover, CsPbBr₃/SiO₂ showed much higher stability compared to bare CsPbBr₃ QDs, when the samples were stored in the humid air (25°C, 75%RH) for 3 days. [4]

Z. Li et al. synthesized CsPbBr₃ QDs that were encapsulated with TiO₂ by adding titanium butoxide (TBOT) as a titanium precursor. TiO₂ shell coating can diminish anion exchange and photodegradation resulting in the enhancement of water stability for more than 3 months, as well as improvement of electrical conductivity, while the bare CsPbBr₃ QDs participated out from toluene can be stable in water only 1 d and their PL was totally quenched after 3 d with structure degradation. Moreover, CsPbBr₃/TiO₂ nanocrystal was tested by mixing PbCl₂ and PbI₂ as Cl and I precursor, respectively, to investigate halide exchanging. The emission peak position and full width at half-maximum (FWHM) remain the same after 15 d. It means that coating TiO₂ on the CsPbBr₃ QDs effectively prevents access of water and halide ions to QDs surface. [2]

Similarly, A. D. Pramata et al. has also used the TiO₂ coating technique for CsPbBr_xI_{3-x} QDs to develop “the reversible on/off switching of luminescence process”. CsPbBr₃ QDs were synthesized by a modified ligand-assisted reprecipitation (LARP) and then, were coated with TiO₂ using titanium tetraisopropoxide (TTIP) as a precursor. The results of CsPbBr₃/TiO₂ nanocrystal showed that it can control the PL emission by transferring the excited electron to polyoxometalates and there is a significant stability improvement of QDs, that can keep 80% of their initial PL intensity after 4 days. Besides the stability, it was proved that coating TiO₂ did not inhibit the charge carrier transfer, and TiO₂ can work as a semiconductor shell [27].

CHAPTER 3

METHODOLOGY

In this chapter, the experiment procedures are divided into 5 parts including the preparation of CsPbBr₃ QDs, encapsulation of CsPbBr₃ QDs with TiO₂ by ex-situ and in-situ method, stability testing at various conditions, characterizations of the samples at different times and photoelectrochemical characterization.

3.1 Preparation of CsPbBr₃ QDs

CsPbBr₃ QDs were synthesized via hot-injection method applied with the three-precursor approach techniques and benzoyl bromide as halide precursors, which were improved from M. Imran et al.

3.1.1 Materials

- 1) Cesium carbonate, Cs₂CO₃ (Wako, 99%)
- 2) Lead acetate trihydrate, Pb(CH₃COO)₂·3H₂O (Wako, 99.99%)
- 3) 1-octadecene, ODE (Wako, 98%)
- 4) Benzoyl bromide, C₆H₅COBr (TCI, 98%)
- 5) Oleic acid, OA (Wako, 99%)
- 6) Oleylamine, OLM (Wako, 95%)
- 7) Toluene (Wako, 99.5%)

3.1.2 Synthesis of CsPbBr₃ QDs

- 1) Cs₂CO₃ (16 mg), Pb(CH₃COO)₂·3H₂O (76 mg), ODE (5.00 mL), OA (0.45 mL) and OLM (1.00 mL) were put in the three-neck flask, stirred at 250 rpm and heated under vacuum at 130°C for 1.40 h. Then, the solution was heated under argon at 170°C for 15 min.
- 2) When the system reached the designed condition, swiftly injected benzoyl bromide 72 μL into the solution. The green solid particles of CsPbBr₃ QDs were formed. Afterwards, immediately cooled down the

solution in an ice-water bath to stop the reaction and waited until the temperature of solution decreased to room temperature (25°C).

- 3) The colloidal solution of CsPbBr₃ QDs was poured into a centrifuge tube and washed by 10 mL toluene, followed by centrifugation at 4,000 rpm for 10 min. The supernatant was discharged. The precipitate was re-dispersed in 10 mL toluene. The centrifugation step was repeated for 2 times to remove the ligands.

3.2 Encapsulation of CsPbBr₃ QDs with TiO₂

For CsPbBr₃/TiO₂, CsPbBr₃ QDs were coated by TiO₂ using TTIP as a titanium precursor via ex-situ and in-situ methods. The effects of encapsulation method on morphology, structural and optical properties of the samples were investigated.

3.2.1 Materials

- 1) CsPbBr₃ QDs in toluene (synthesized via hot-injection method)
- 2) Titanium tetraisopropoxide, TTIP (Wako, 97%)
- 3) Toluene (Wako, 99.5%)

3.2.2 Synthesis of CsPbBr₃/TiO₂ by ex-situ method

- 1) 60 μ L TTIP dissolved in 1 mL toluene (0.067 M) was added dropwise into 10 mL colloidal solution of CsPbBr₃ QDs dissolved in toluene (0.10 M), and then stirred at room temperature and 30%RH for 2 h.
- 2) The colloidal CsPbBr₃/TiO₂ solution was collected in a centrifuge tube and centrifuged at 4,000 rpm for 10 min to separate the precipitate of CsPbBr₃/TiO₂ nanocrystals.

3.2.3 Synthesis of CsPbBr₃/TiO₂ by in-situ method

- 1) After injection of benzoyl bromide in the step of CsPbBr₃ QDs synthesis, the 60 μ L of TTIP was directly injected into the solution at different temperatures (170°C, 100°C and 25°C), while the system was cooling down in an ice-water bath.

- 2) The solution was stirred at room temperature and 30%RH for 2 h.
- 3) The colloidal CsPbBr₃/TiO₂ solution was collected by toluene and centrifuged at 4,000 rpm for 10 min. The precipitate was re-dispersed in 10 mL toluene. The centrifugation step was repeated for 2 times to remove the ligands.

3.3 Stability testing

To investigate the stability of bare CsPbBr₃ QDs and CsPbBr₃/TiO₂ synthesized via ex-situ and in-situ methods, the samples were stored under different conditions as shown in table 3.1. The stability of the dried samples which were stored under ambient air for 5 days was monitored by the change in crystallinity calculated from XRD results at day 0, 2 and 5. Then, the samples were dispersed in toluene to investigate the change in PL intensity with an excitation wavelength at 365 nm. To test the stability against water, the samples were dried under vacuum for 10 min and dispersed in DI water with ultrasonication treatment for 30 min. A LED light (Optocode Corporation, LED455/L-STND) was applied as a source of visible light at 455 nm (80 mW) to test the stability of the samples dispersed in toluene under continuous visible light illumination for 80 min. The method for measuring the water and photostability was the same as the case of toluene.

Table 3.1 Storage conditions of the samples.

Testing conditions	Media	Time range
1) Ambient air (70%RH, 28°C)	Powder form	5 days
2) Non-polar solvent (25°C)	Toluene	7 days
3) Water with ultrasonication (25°C)	Deionized water	30 min
4) Visible light illumination (455 nm, 80 mW)	Toluene	80 min

3.4 Characterization of the samples

The Fourier Transform Infrared spectrophotometer (FT-IR, FT/IR-4100, JASCO Co.) was employed to investigate the ligand removal of the samples before testing the stability. The size and morphology of the samples were observed by transmission electron microscope (TEM-2000FX, JEOL). The crystallinity was determined by X-ray diffraction (RINT2100, Rigaku Co., Ltd) with $\text{CuK}\alpha$ radiation source in the range of 10-60° and a scan rate of 10 deg/min. The optical properties were studied by using a UV-Visible spectrophotometer (V-650, JASCO Co.) at the wavelength range of 350-700 nm. Steady state PL spectra and quantum yields of QDs were obtained with a spectrometer (FP-6000, JASCO Co.) with an excitation at 365 nm. The elemental composition of materials was determined by using X-ray fluorescence spectrometer (XRF, ZSX Primus II, Rigaku Co., Ltd.).

3.5 Photoelectrochemical characterization

In order to investigate the improvement of charge transport properties after encapsulation of CsPbBr_3 QDs with TiO_2 , the photoelectrochemical was applied and the characteristics of cyclic voltammetry and current-voltage curve was considered.

3.5.1 Cyclic voltammetry (CV)

To study the reduction and oxidation of the samples in PEC cell, the cyclic voltammetry (CV) measurement with potentials scanned between -1.7 and 1.7 V (vs. Ag/AgNO_3) and the sweep rate of $10 \text{ mV}\cdot\text{s}^{-1}$ was carried out with a standard three-electrode setup by using FTO ($2 \times 2 \text{ cm}^2$) as a working electrode, a Pt mesh as a counter electrode and Ag/AgNO_3 wire as a reference electrode. The bare CsPbBr_3 QDs and the $\text{CsPbBr}_3/\text{TiO}_2$ samples were dispersed in the electrolyte solution containing 0.1 M TBAPF_6 in 15 mL acetonitrile. The light source was 455 nm LED light (Optocode Corporation, LED455/L-STND). The system was shown in figure 3.1.

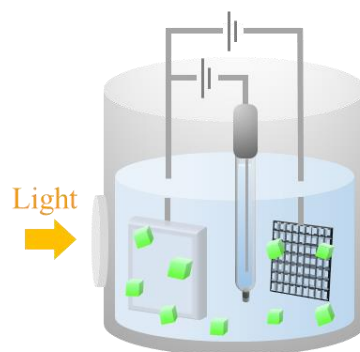


Figure 3.1 Standard three-electrode setup for CV measurement.

3.5.2 Current-voltage (IV) characteristics

To investigate the performance of the samples in PEC cell, the current-voltage (IV) curves were performed with potentials scanned from 0 to 0.10 V (vs. Ag/AgNO₃) and the sweep rate of 10 mV.s⁻¹ by using three-electrode system with two-compartments separated by nafion membrane (figure 3.2), which added methanol as electron donor in anode site and polyoxometalates (POM) as electron acceptor in cathode site. The samples were dispersed in the electrolyte solution containing 0.1 M TBAPF₆ in 15 mL acetonitrile. The FTO (2x2 cm²), Pt mesh and Ag/AgNO₃ wire were used as a working electrode, a counter electrode and a reference electrode, respectively. The 455 nm LED light was applied to the anode site to induce the charge generation in CsPbBr₃ QDs. Since POM⁻ can be reoxidized to POM by oxygen, the argon was continuously purged into the POM solution.

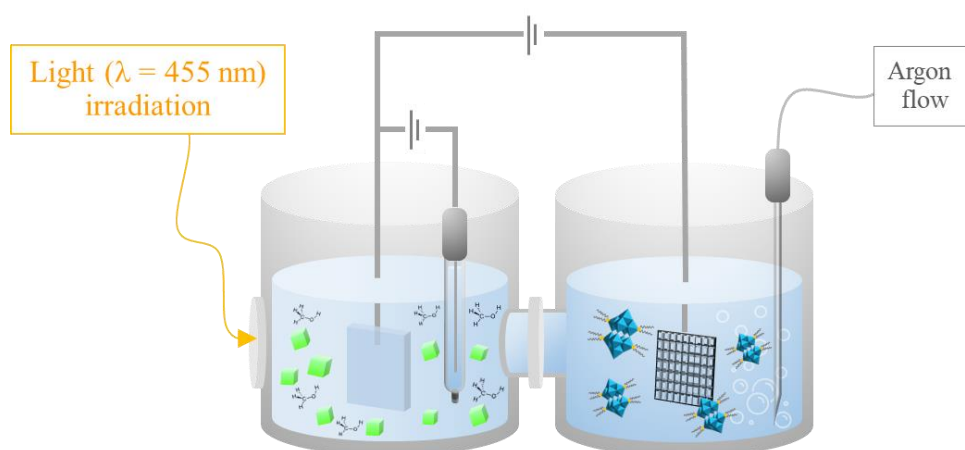


Figure 3.2 The PEC setup for IV measurement.

CHAPTER 4

RESULTS AND DISCUSSION

Herein, we investigated the optimum conditions for encapsulation process of CsPbBr₃/TiO₂ to enhance the stability of CsPbBr₃ QDs. The stability of CsPbBr₃/TiO₂ was tested under ambient air, toluene, water and light. Finally, the charge transport property was characterized by using as a photoelectrochemical cell.

4.1 Effects of ligand removal processes

In this study, the CsPbBr₃ QDs were obtained by hot-injection method which used the long carbon chain organic ligands including oleic acid (OA) and oleylamine (OLM) to control the growth and stabilize the CsPbBr₃ QDs during the synthesis process. However, these ligands prevented charge transfer as an insulating shell in optoelectronic devices; moreover, they also had an influence in the properties of QDs as shown in figure 4.1. Therefore, these ligands should be removed from the samples before investigation of their performance. The common ligand removal technique was centrifugation followed by washing with nonpolar solvent to separate the QDs and ligands. However, the multiple washes resulted in a mass loss of the QDs, so the number of washing cycles was considered in the study.

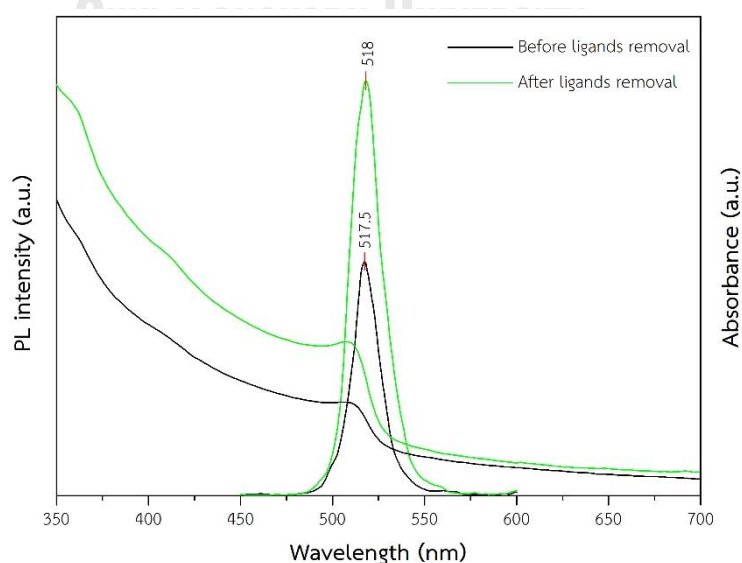


Figure 4.1 PL emission spectra of CsPbBr₃ QDs before and after ligand removal.

The FT-IR peaks of these ligands was observed before and after ligand removal process as shown in figure 4.2. FT-IR spectra showed that there are characteristic modes of oleyl groups corresponding to the OA and OLM as follows: peaks at $2,924\text{ cm}^{-1}$ and $2,854\text{ cm}^{-1}$ correlate with the asymmetric and symmetric CH stretching mode in both OA and OLM, respectively, and peaks at $1,462\text{ cm}^{-1}$ and $1,376\text{ cm}^{-1}$ correlate with the CH_2 and CH_3 bending in OLM, respectively [28]. After washing, the large amount of ligand was significantly removed until the second centrifugation in which the area of FT-IR peak decreased by 95% of its initial value.

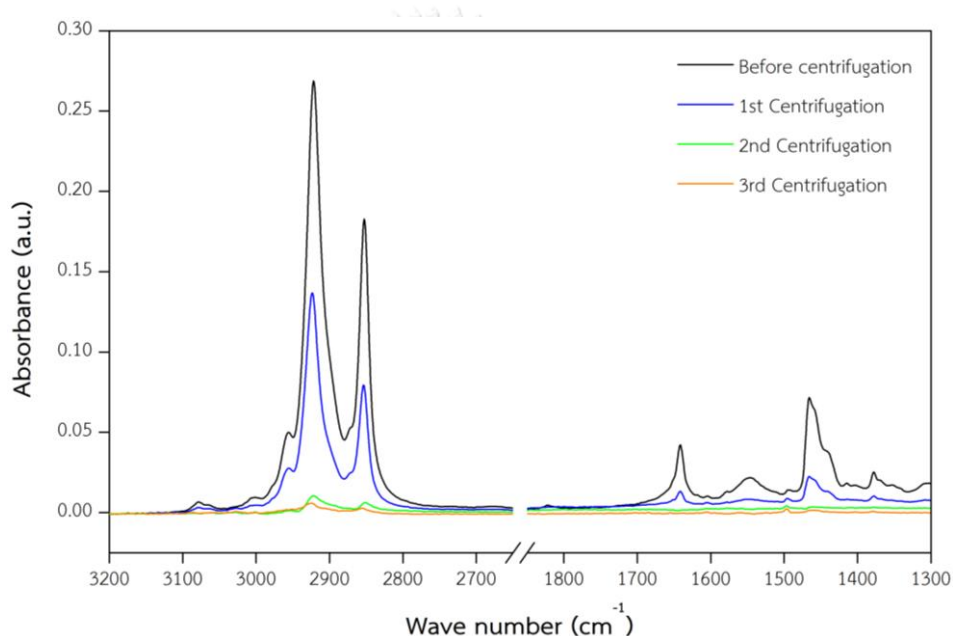


Figure 4.2 FT-IR of CsPbBr_3 QDs before and after centrifugation at different times.

After multiple washing cycles, there was no significant difference in amount of ligand because the remaining ligands were difficult to remove by this technique, while the mass of QDs still lost during the process (figure 4.3). Consequently, washing cycles for 2 times was the most suitable condition for the sample treatment before characterization. Therefore, bare CsPbBr_3 QDs and $\text{CsPbBr}_3/\text{TiO}_2$ from in-situ method were washed after synthesis and encapsulation for 2 times. While $\text{CsPbBr}_3/\text{TiO}_2$ from ex-situ method was washed before encapsulation process for 2 times to remove the ligands before the analysis. However, to get more details of the residual ligand content, the atomic percentage of carbon can be measured with the X-ray photoelectron spectroscopy (XPS) in the further study.

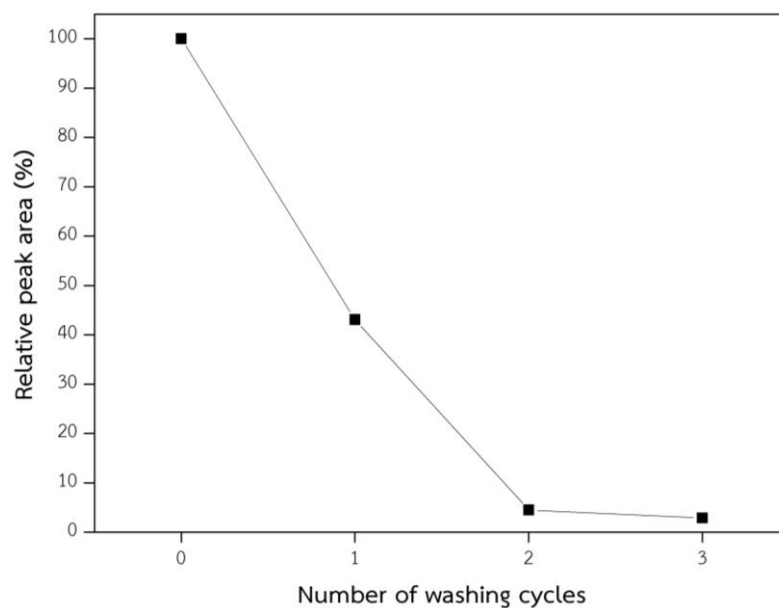


Figure 4.3 Relative FT-IR peak area of ligands at different washing cycles.

The FT-IR results of all samples after ligand removal (figure 4.4) showed that most of ligands were separated into the supernatant. Moreover, the amount of ligand in each sample was almost the same and less than 5% of before ligand removal.

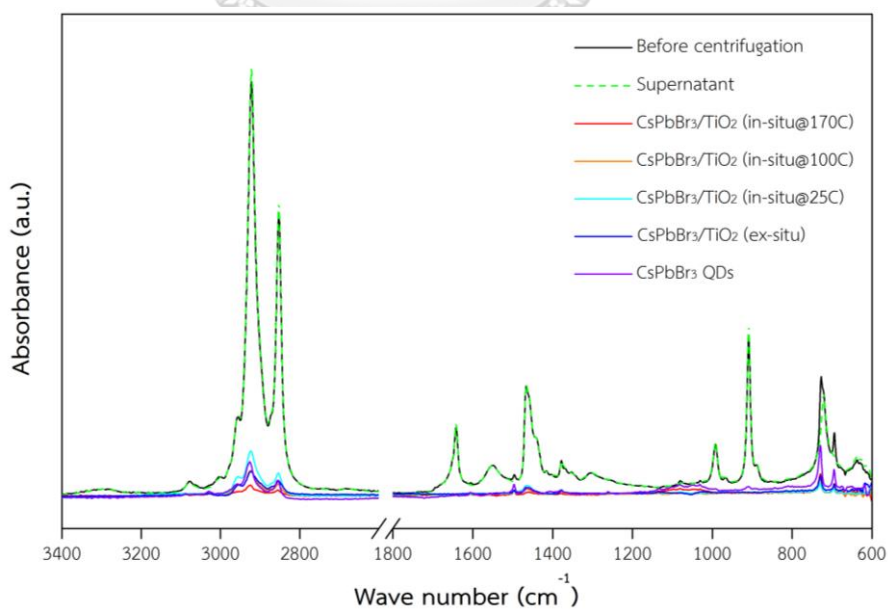


Figure 4.4 FT-IR spectra of the samples before and after centrifugation.

4.2 Morphology and structure of bare CsPbBr₃ QDs and CsPbBr₃/TiO₂

The morphology, element compositions and structural properties of bare CsPbBr₃ QDs and CsPbBr₃/TiO₂ prepared by ex-situ and in-situ encapsulation processes were investigated using TEM, XRF and XRD.

4.2.1 Morphology and particle size distribution

CsPbBr₃ QDs were synthesized via hot-injection method improved from M. Imran et al. to obtain the nanocrystals with an orthorhombic phase. The bare CsPbBr₃ QDs exhibited a uniform cubic shape with a narrow size distribution and the average size of 14.08 nm (figure 4.5). After coating CsPbBr₃ QDs with TiO₂ by in-situ method, all samples showed cubic-shape nanoparticles with dark spots of TiO₂ on their surface (figure 4.6, figure 4.7, figure 4.8). The average size of CsPbBr₃/TiO₂ coated by in-situ method and injected TTIP at 170°C, 100°C and 25°C were 11.78, 12.55 and 13.34 nm, respectively. However, CsPbBr₃/TiO₂ coated by ex-situ method exhibited an agglomeration of QDs surrounding with gray shadow area of TiO₂ (figure 4.9) in which the size of an agglomerated cluster in TEM results was around 200-540 nm measured by the image processing program, Image J. The agglomeration of CsPbBr₃/TiO₂ was due to the strong ionic nature between the uncapped QDs of neighboring particles as well as between the oxide of titanium. The ligands in ex-situ sample were removed before coating with TiO₂ so the QDs had coagulated since the step of ligand removal, then the step of encapsulation activated more agglomeration between uncapped QDs by oxide of titanium.

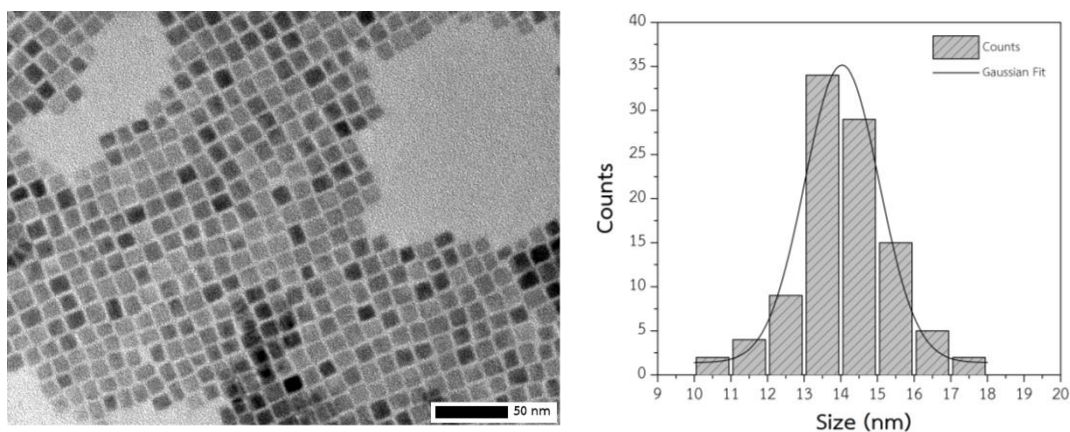


Figure 4.5 TEM image and size distribution histogram of bare CsPbBr_3 QDs synthesized via hot-injection method.

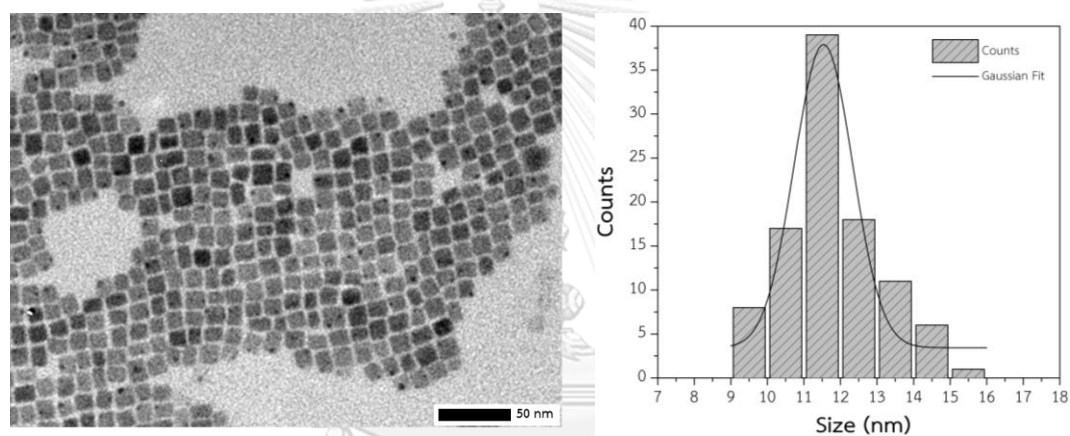


Figure 4.6 TEM image and size distribution histogram of $\text{CsPbBr}_3/\text{TiO}_2$ coated by in-situ method and injected TTIP at 170°C .

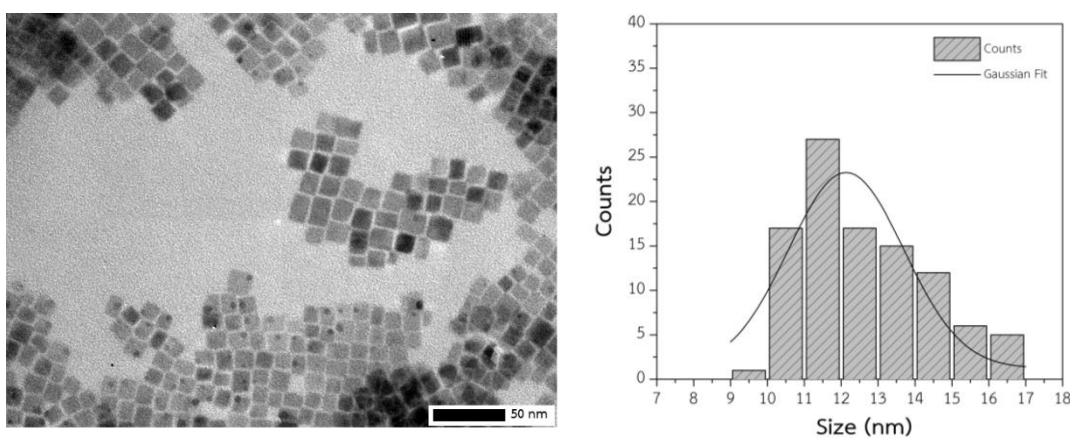


Figure 4.7 TEM image and size distribution histogram of $\text{CsPbBr}_3/\text{TiO}_2$ coated by in-situ method and injected TTIP at 100°C .

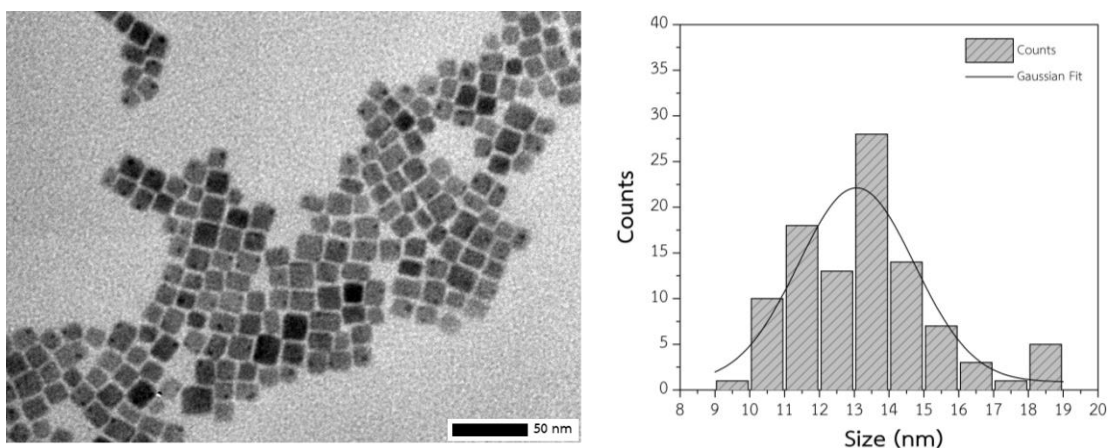


Figure 4.8 TEM image and size distribution histogram of CsPbBr₃/TiO₂ coated by in-situ method and injected TTIP at 25°C.

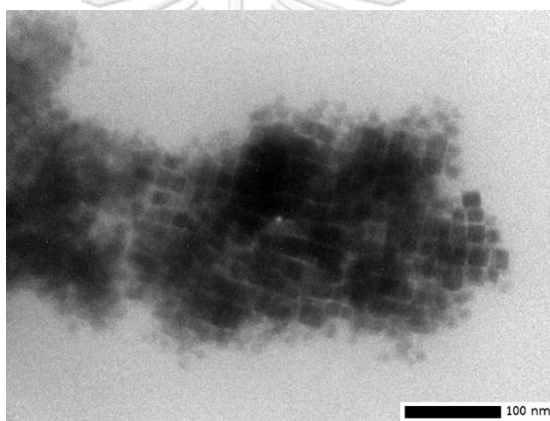


Figure 4.9 TEM image of CsPbBr₃/TiO₂ coated by ex-situ method.

4.2.2 Elemental and chemical composition

The chemical compositions of the samples were measured by X-ray fluorescence spectrometer to study the effects of encapsulation method on the amount of coated TiO₂. Table 4.1 shows the molar compositional ratio of Cs, Pb, Br and Ti elements. The results show that the molar ratio of Pb : Br was around 1 : 3. However, the molar ratio of the samples did not follow the chemical formula of CsPbBr₃. The detected Cs element was less than theoretical values since Cs⁺ possibly did not engage in strong chemical bonding with octahedral PbBr₆⁻, where covalent bonds between Pb and Br atoms are the major interactions. When comparing the

molar Cs : Ti ratio among samples, the ex-situ coated sample exhibited the largest amount of Ti on CsPbBr₃ QDs (Cs : Ti ratio 1 : 3.50). The multiple-steps of ex-situ method could cause the higher humidity of the solution compared to the controllable conditions of the one-step method so the TTIP precursor was easily hydrolyzed to TiO₂. In addition, the TTIP was not hindered by the ligands surrounding the QDs so more amount of TTIP could be adsorbed on the QDs surface. While the molar Cs : Ti ratios of in-situ coated samples at 170°C, 100°C and 25°C were 1 : 0.02, 1 : 0.15 and 1 : 0.10, respectively since the effects of the ligand-restricted adsorption of TiO₂ caused the less Ti ratio. Furthermore, immediately injecting TTIP at 170°C might interrupt the formation of QDs and the adsorption of TTIP on their surface.

Table 4.1 The molar compositional ratio of Cs : Pb : Br : Ti of the five samples.

Samples	Molar compositional ratio of Cs : Pb : Br : Ti			
	Cs	Pb	Br	Ti
Bare CsPbBr ₃ QDs	1	6.2	18.6	0
CsPbBr ₃ /TiO ₂ (ex-situ)	1	3.9	12.2	3.50
CsPbBr ₃ /TiO ₂ (in-situ at 170°C)	1	2.9	9.6	0.02
CsPbBr ₃ /TiO ₂ (in-situ at 100°C)	1	4.1	12.9	0.15
CsPbBr ₃ /TiO ₂ (in-situ at 25°C)	1	2.7	8.9	0.10

4.2.3 Structural properties

The CsPbBr₃ QDs exhibited the split diffraction peak at 15.3°, which was the characteristic pattern of orthorhombic phase corresponding to (002) and (110) planes, as well as a diffraction peak at $2\theta = 21.5^\circ$ and 30.5° assigning to the orthorhombic planes of (112) and (220) as shown in the XRD result (figure 4.10). After encapsulation by titanium precursor, XRD patterns were also recorded to investigate any changes that might have occurred in the phase or crystallite sizes of the CsPbBr₃ QDs. It was observed that the orthorhombic phase of QDs remained preserved, and the impurity

phase was not generated after coating with TiO_2 . The crystallite size of the peaks was calculated and given in table 4.2. These values corresponded to the TEM results except the ex-situ coated sample, which the cluster of QDs was occurred in TEM. It was obvious that the TiO_2 encapsulation process caused the decrease of crystallite size. Adding TTIP precursor during formation of QDs at higher temperature could hinder the growth of QDs and cause the smaller crystallite size. In addition, it has been reported that the QDs surface could react with a trace of water produced from the TiO_2 synthesis and it caused partially dissolving of outer surface [2]. Therefore, the crystal size of ex-situ coated sample was smallest due to the largest amount of TiO_2 , although there was an agglomeration of QDs leading to a large cluster.

In terms of crystallinity, the crystallinity was improved after coating with TiO_2 by ex-situ and in-situ method since TiO_2 could slow the growth process of QDs in which facilitated the crystallization and the formation of highly crystalline CsPbBr_3 QDs. Nevertheless, when compared among the in-situ coated samples, the higher TTIP injection temperature interrupted the growth of some crystal faces as observed in XRD patterns resulting in a lower degree of crystallinity.

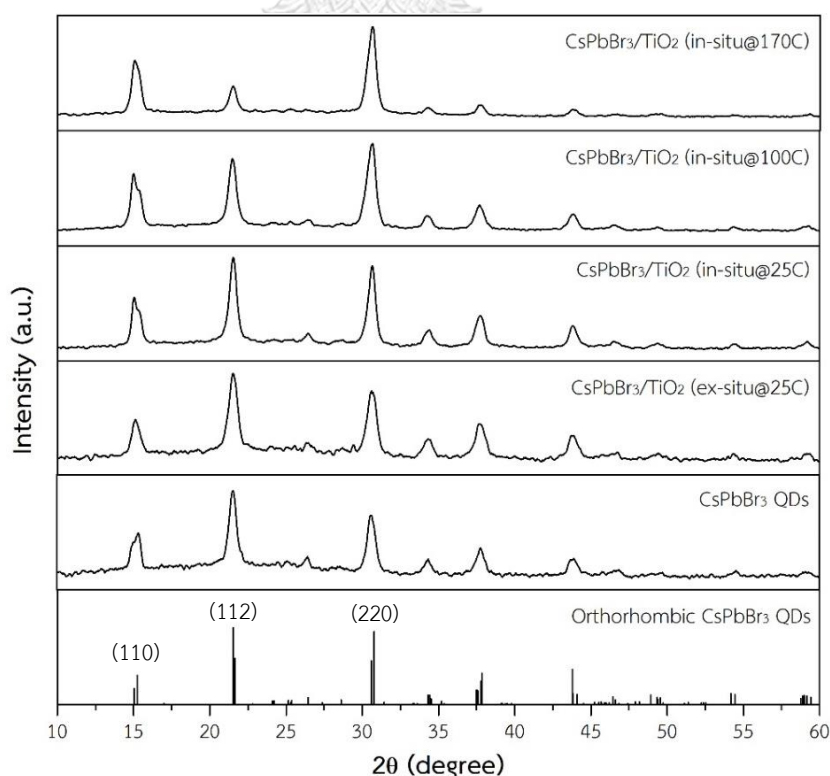


Figure 4.10 XRD pattern of CsPbBr_3 QDs and $\text{CsPbBr}_3/\text{TiO}_2$ by various methods.

Table 4.2 Crystallite size and crystallinity calculated from XRD results.

Samples	Crystallite size (nm)	Crystallinity (%)
Bare CsPbBr ₃ QDs	13.16 ± 0.49	35.63
CsPbBr ₃ /TiO ₂ (in-situ at 25°C)	12.82 ± 0.66	52.10
CsPbBr ₃ /TiO ₂ (in-situ at 100°C)	12.28 ± 0.66	47.32
CsPbBr ₃ /TiO ₂ (in-situ at 170°C)	11.12 ± 0.79	45.52
CsPbBr ₃ /TiO ₂ (ex-situ)	10.07 ± 0.44	44.55

Besides the effects of TiO₂ on the crystal size of QDs, the encapsulation process also affected the crystal faces. In fact, XRD relative intensity of (112) to (220) face became smaller as the TTIP injection temperature increased (figure 4.11). In contrast, XRD relative intensity of (110) to (220) face kept constant. This result ensured that (110) and (220) faces grew together without interference of TTIP injection, while the growth of (112) face was hindered at high injection temperature.

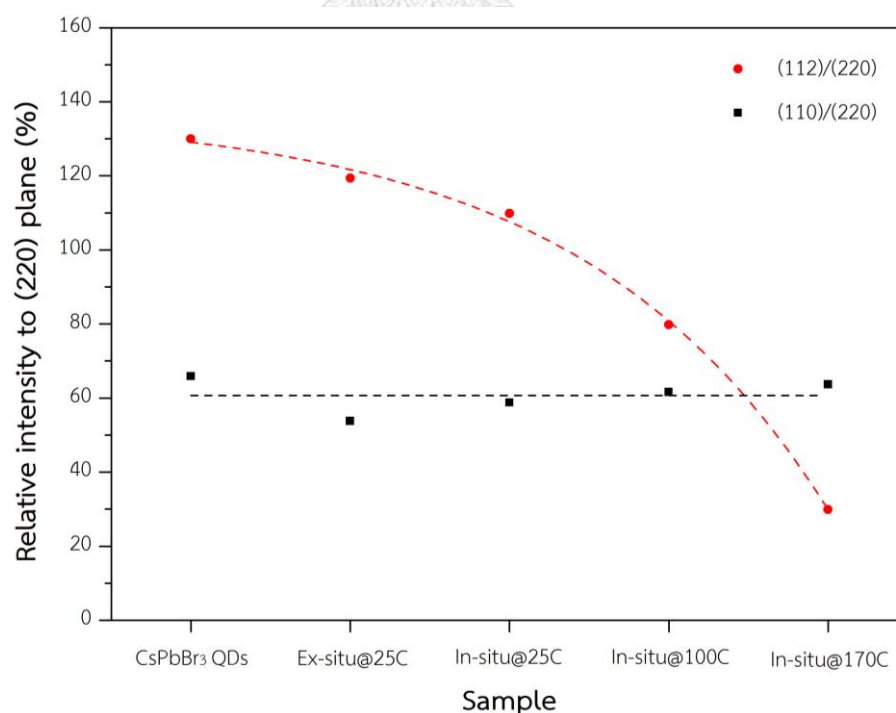


Figure 4.11 The relationship between XRD relative intensity of (112) and (110) face to (220) face and the samples synthesized by different methods.

4.3 Optical properties of bare CsPbBr₃ QDs and CsPbBr₃/TiO₂

To investigate the effects of encapsulation process on the optical properties of CsPbBr₃ QDs, the PL emission spectra and UV-Visible absorption were studied, as shown in figure 4.13. The CsPbBr₃ QDs exhibited green emissions and a sharp emission peak at wavelength 515 nm (2.41 eV) with a full width at half maximum (FWHM) of 16 nm when excited at 365 nm (3.40 eV). After coating CsPbBr₃ QDs with titanium precursor by in-situ method, the PL peaks of the in-situ samples at 170°C, 100°C and 25°C were 515 nm (2.41 eV), 516 nm (2.40 eV) and 516 (2.40 eV) with a FWHM of 18 nm, 17 nm and 17 nm, respectively. However, the emission peak of CsPbBr₃/TiO₂ coated by ex-situ method shifted from 515 to 518 nm (2.39 eV) with a FWHM of 16 nm. We can observe with the naked eyes that the color changed from green particle of CsPbBr₃ QDs to yellow particle of CsPbBr₃/TiO₂. The red-shift of PL emission peak corresponded to the agglomeration of QDs as a cluster.

The bandgap of CsPbBr₃ QDs and CsPbBr₃/TiO₂ coated by in-situ and ex-situ methods were summarized in table 4.3. The bandgap of bare CsPbBr₃ QDs was about 2.39 eV in which the result was agreed with previous study. Moreover, the same bandgap of 2.39 eV also occurred in the in-situ coated sample at 25°C and 100°C. However, the in-situ coated sample at 170°C and ex-situ coated sample exhibited a lower bandgap of 2.35 and 2.33 eV, respectively. The defects in the structure and large particle size could decrease the bandgap of these sample.

Table 4.3 The bandgap of the five samples.

Sample	Bandgap (eV)
Bare CsPbBr ₃ QDs	2.39
CsPbBr ₃ /TiO ₂ (in-situ at 25°C)	2.39
CsPbBr ₃ /TiO ₂ (in-situ at 100°C)	2.39
CsPbBr ₃ /TiO ₂ (in-situ at 170°C)	2.35
CsPbBr ₃ /TiO ₂ (ex-situ)	2.33

Furthermore, the encapsulation process can affect the photoluminescence quantum yield (PLQY) of CsPbBr₃/TiO₂ as shown in figure 4.12. The bare CsPbBr₃ QDs exhibited the highest PLQY at 98.5%. However, after TiO₂ coating, the samples showed a decrease of PLQY. The PLQY of the in-situ samples at 170°C, 100°C and 25°C were 93.5%, 72.1% and 80.6%, respectively, while the PLQY of the ex-situ sample was lowest at 1.3%. When considered the relationship between the PLQY and amount of Ti on the in-situ coated samples, we found that the PLQY linearly decreased as amount of Ti increased. It can be explained that the conduction band minimum level of amorphous TiO₂ was lower than the lowest unoccupied molecular orbital of CsPbBr₃ QDs so the electron can delocalize over the CsPbBr₃ QDs and coated TiO₂, which could facilitate the charge transfer and quench PL intensity leading to decrease of the PLQY.

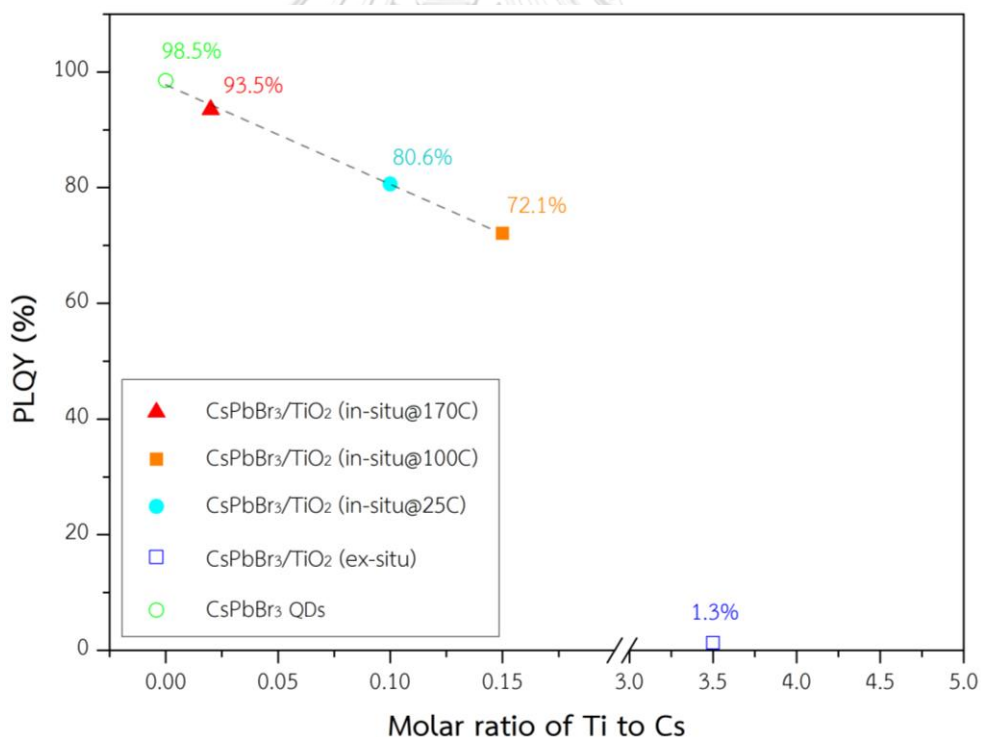


Figure 4.12 The relationship between PLQY (%) and molar ration of Ti to Cs.

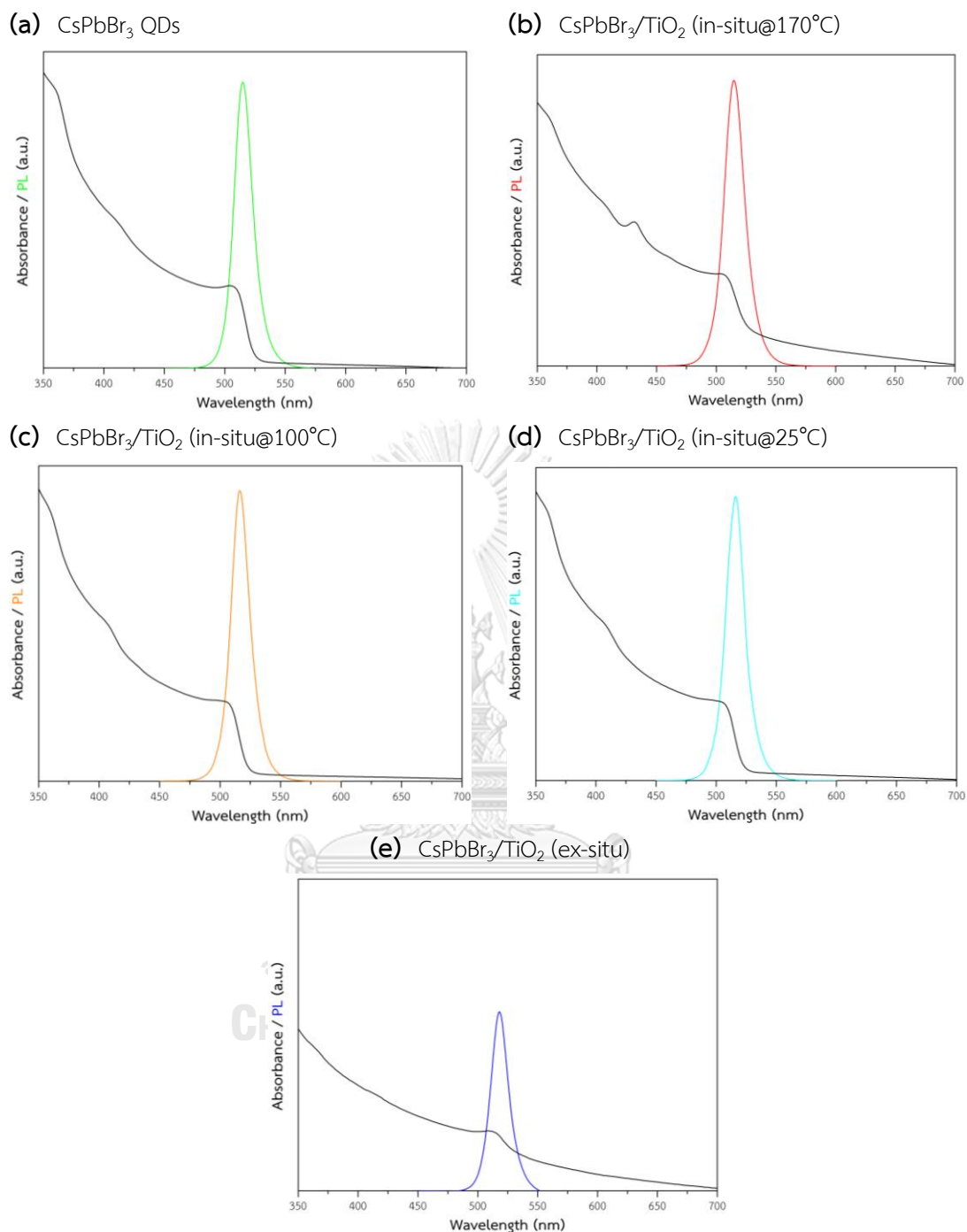


Figure 4.13 PL emission spectra and UV-Visible absorption of (a) CsPbBr₃ QDs, CsPbBr₃/TiO₂ coated by in-situ method (b) at 170°C (c) at 100°C (d) at 25°C and by (e) ex-situ method. The excitation wavelength was 365 nm.

4.4 Stability testing

In order to investigate the stability of CsPbBr₃/TiO₂ coated by different methods, the samples were stored under different conditions consisting of ambient air, toluene, DI water and light illumination.

4.4.1 Ambient air

XRD pattern was used to monitor the evolution of QDs structure while the sample powder was being kept under ambient air. The relative crystallinity (figure 4.14) and XRD results of CsPbBr₃ QDs (figure 4.15) showed a peak splitting and a rapid decline in crystallinity to 85% of its initial value within 5 days. A loss of perovskite crystallinity indicated a loss in long range order and becoming structurally amorphous, corresponding a reduction in structural stability. It is possible that the environment factors such as light, oxygen and humidity had destroyed their structure and induced amorphization of crystals as studied in previous research [29]. In contrast, all CsPbBr₃/TiO₂ samples under ambient condition showed much higher stability in which the crystallinities were more than 90% of their initial values after 5 days. In addition, the ex-situ coated sample exhibited the most excellent stability in powder form owing to the largest amount of TiO₂ coated on QDs surface.

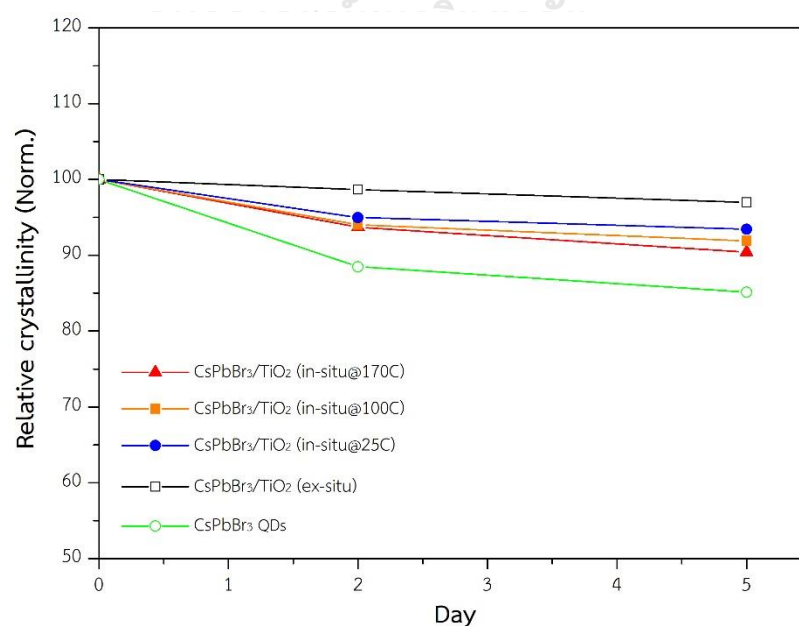


Figure 4.14 The comparison of calculated crystallinity for the five samples under air.

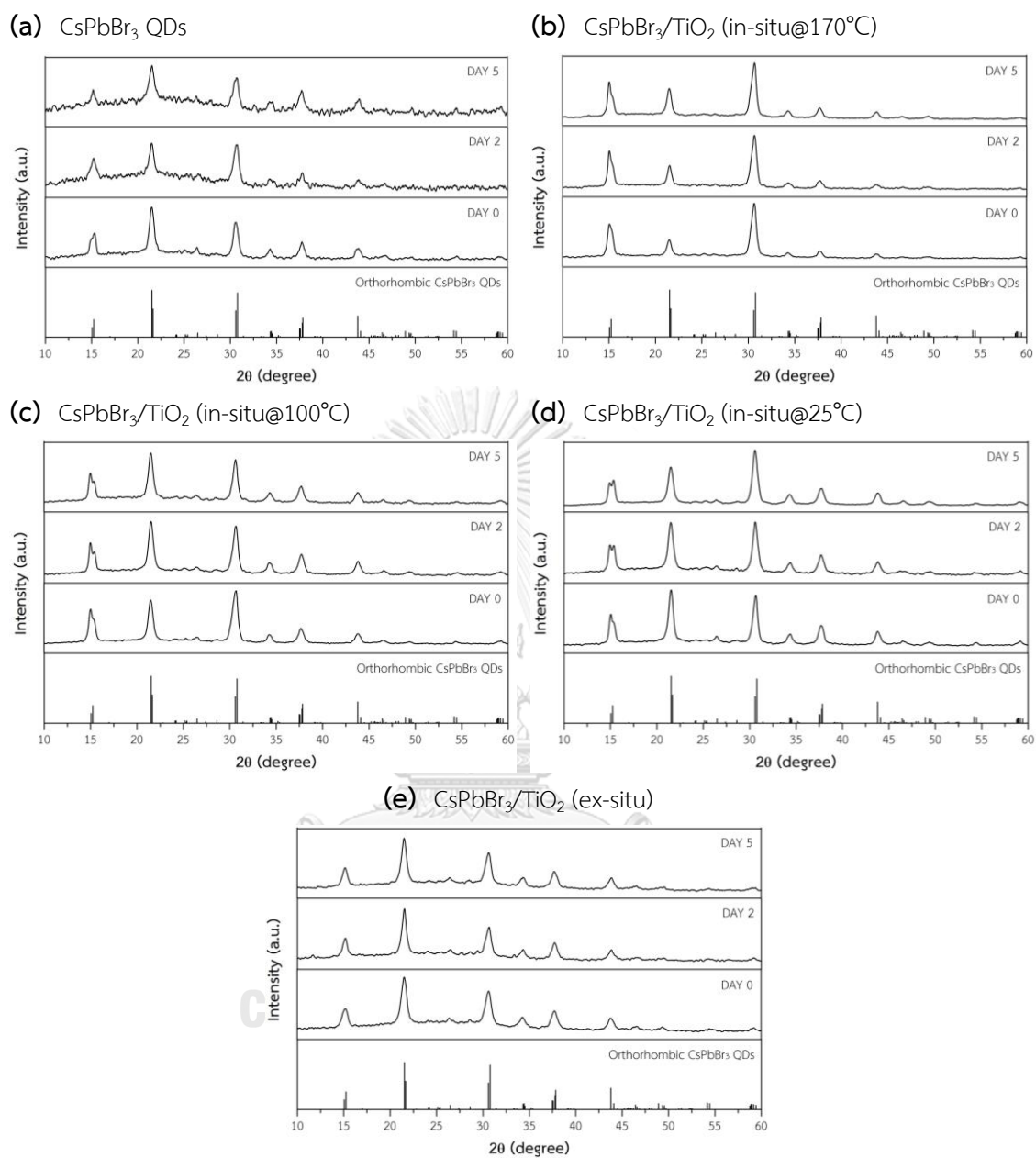


Figure 4.15 Stability of (a) CsPbBr₃ QDs, CsPbBr₃/TiO₂ coated by in-situ method (b) at 170°C (c) at 100°C (d) at 25°C and by (e) ex-situ method, which were stored under ambient air in powder form.

4.4.2 Toluene

Toluene was widely used as a solvent for synthesis and characterization of CsPbBr₃ QDs in many studies [2, 4, 5, 29] because this common nonpolar solvent can disperse QDs very well and not interrupt charge transfer process [30]. Nevertheless, the long-term instability of bare QDs in toluene was still a problem due to its intrinsic factors as well as extrinsic factors such as a trace of water in solvent media. In order to investigate the stability improvement of CsPbBr₃/TiO₂, the samples were dispersed in toluene and monitored the change in PL intensity for 7 days. The relative PL intensity (figure 4.16) of five samples showed that the ex-situ coated CsPbBr₃ QDs in toluene was totally decreased in the PL after 5 days, while the bare CsPbBr₃ QDs had a slower degradation rate, although its PL was quenched to 46% within 1 week. It indicated that the ex-situ and bare CsPbBr₃ QDs could be aggregated easier in solution. However, the in-situ coated samples showed an excellent PL stability and can maintain their PL intensity of more than 80%. Therefore, the in-situ method was the most suitable strategy to enhance the stability of QDs in toluene, which did not affect their optical properties during preservation.

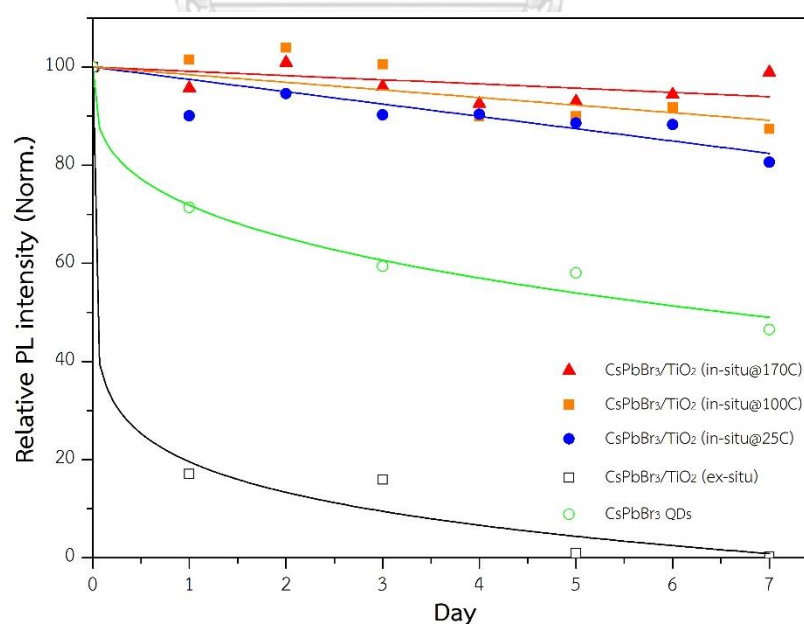


Figure 4.16 The comparison of relative PL intensity for the five samples in toluene.

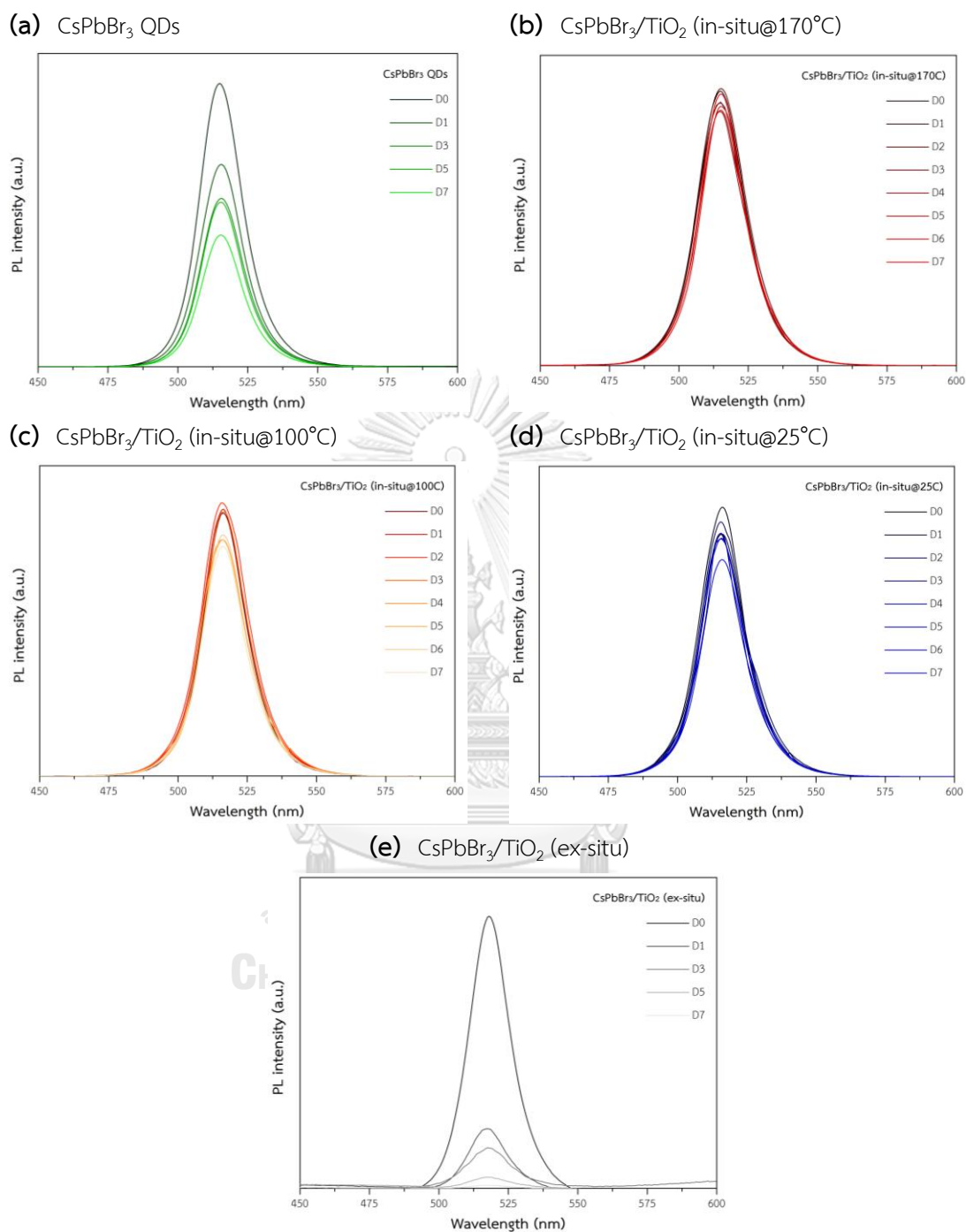


Figure 4.17 Stability of (a) CsPbBr₃ QDs, CsPbBr₃/TiO₂ coated by in-situ method (b) at 170°C (c) at 100°C (d) at 25°C and by (e) ex-situ method, which were stored in non-polar solvent (toluene).

4.4.3 Deionized water with ultrasonication

In order to investigate the enhanced stability of CsPbBr₃/TiO₂ against water, five samples were dispersed in deionized water (DIW). However, there were still remaining hydrophobic ligands of OA and OLM surrounding the QDs surface. Consequently, the dispersion of these samples in DIW was not uniform and partially precipitated. To solve this problem, the ultrasonication treatment was used during the stability. A degradation profile of five samples dispersed in DIW as function of times (figure 4.19) can be fitted with four parameter logistic curve (4PL) to clarify the decomposition mechanism of CsPbBr₃ QDs and CsPbBr₃/TiO₂ in DIW. The pattern of graph can be provided into 3 parts. Firstly, the relative PL intensity remained steady. Then, there was a rapid fall. After, the PL reached a plateau. However, some samples cannot maintain stable at the beginning. This phenomenon can be explained that TiO₂ can protect QDs from DIW for a while before DIW reached and destroyed their uncoated surface. In addition, some TiO₂ could be removed from the QDs surface due to the ultrasonication. Until the water completely destroyed the uncoated particles or all particles (in case of ~0% PL), then the PL intensity became steady.

It was obvious that the relative PL intensity of bare CsPbBr₃ QDs decreased dramatically to 5% within 15 min, and there was a red-shift of PL spectra for 8.5 nm because of the serious aggregation of uncapped QDs. However, the ex-situ sample showed the faster degradation rate, compared with bare QDs, although the ex-situ coated sample exhibited the largest amount of Ti on its surface. It could be due to the particle agglomeration happening during the coating step, which resulted in the structure instability. For the in-situ coated samples, the temperature at 25°C was the best condition for injecting TiO₂ precursor, since the CsPbBr₃/TiO₂ at 25°C can maintain the PL intensity at more than 80% for first 10 min, while the relative PL intensity of the samples coated at 100°C and 170°C dramatically dropped to 60% and 30%, respectively. It can be concluded that both structural properties and amount of TiO₂ after encapsulation was important to the stability of CsPbBr₃ QDs because the CsPbBr₃/TiO₂ at 25°C exhibited both less defects and large amount of Ti, which resulted in a good water stability.

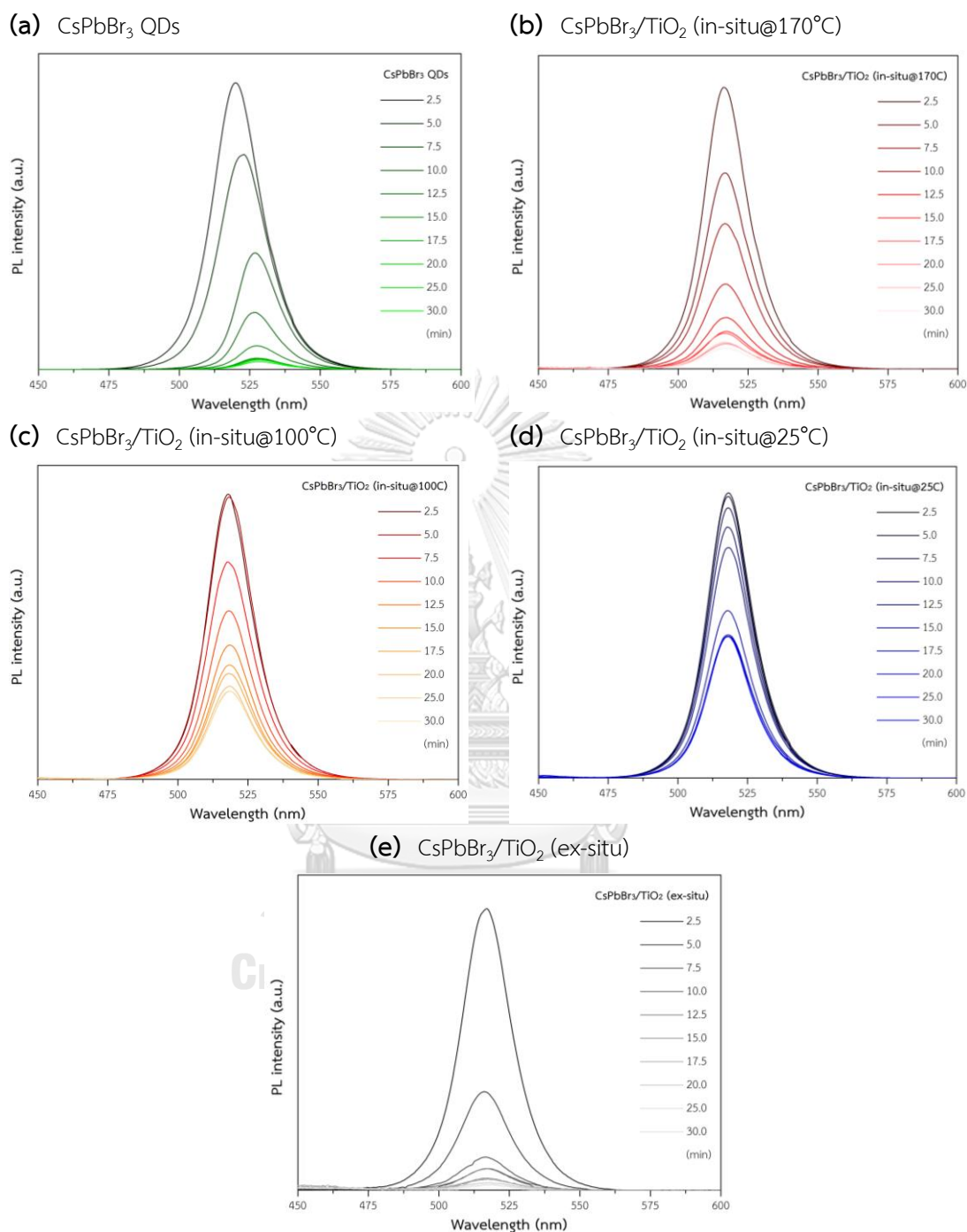


Figure 4.18 Water stability of (a) CsPbBr₃ QDs, CsPbBr₃/TiO₂ coated by in-situ method (b) at 170°C (c) at 100°C (d) at 25°C and by (e) ex-situ method, which were ultrasonicated in DIW.

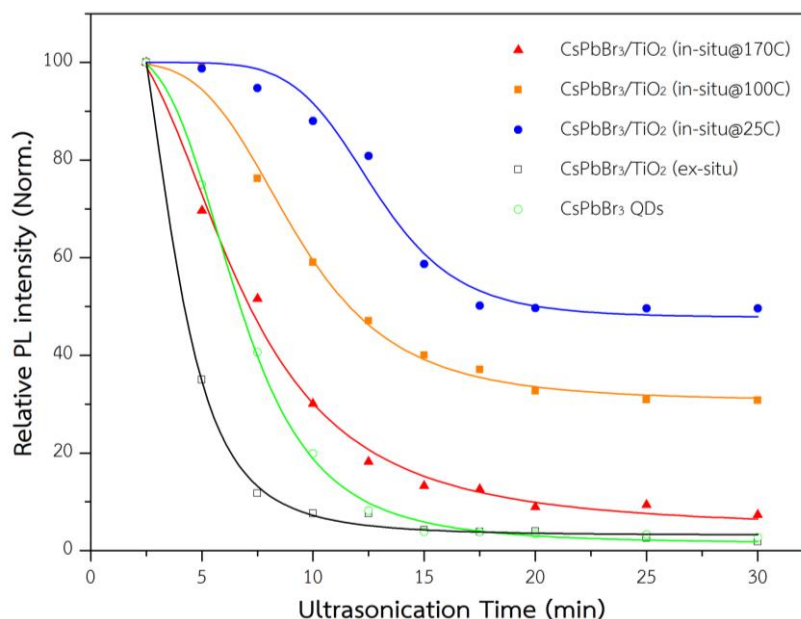


Figure 4.19 The comparison of relative PL intensity for the five samples in DIW.

4.4.4 Light illumination

Although CsPbBr₃ QDs had good optical properties, the photo instability was a serious issue for their working devices. Therefore, the photostability of CsPbBr₃ QDs and CsPbBr₃/TiO₂ in toluene was monitored under visible light irradiation at 455 nm. The PL intensity of bare CsPbBr₃ QDs gradually decreased to 30% after 80 min (figure 4.20a) but there was a red-shifted PL spectrum of 3.5 nm due to the aggregation and elongation of the QDs. Since the light excitation generated charges which can diffuse to the surface, the surrounding ligands captured the charges and was removed into the solution leading to the trap sites and detaching of uncapped QDs [29].

The ex-situ coated CsPbBr₃/TiO₂ (figure 4.20e) was still unstable under light irradiation. However, the in-situ coated CsPbBr₃/TiO₂ samples (figure 4.20b-d) can maintain their PL intensity at $\approx 100\%$ for first 10 min. This result indicated that the in-situ coating method was an effective strategy for improving long-term photostability of CsPbBr₃ QDs due to the tightly bonded agents of TiO₂ passivating the QDs surface in which can protect the formation of trap sites on QDs surface. Moreover, the sample coated at 25°C exhibited the most excellent stability against light illumination according to a good structure and large amount of TiO₂ on its surface.

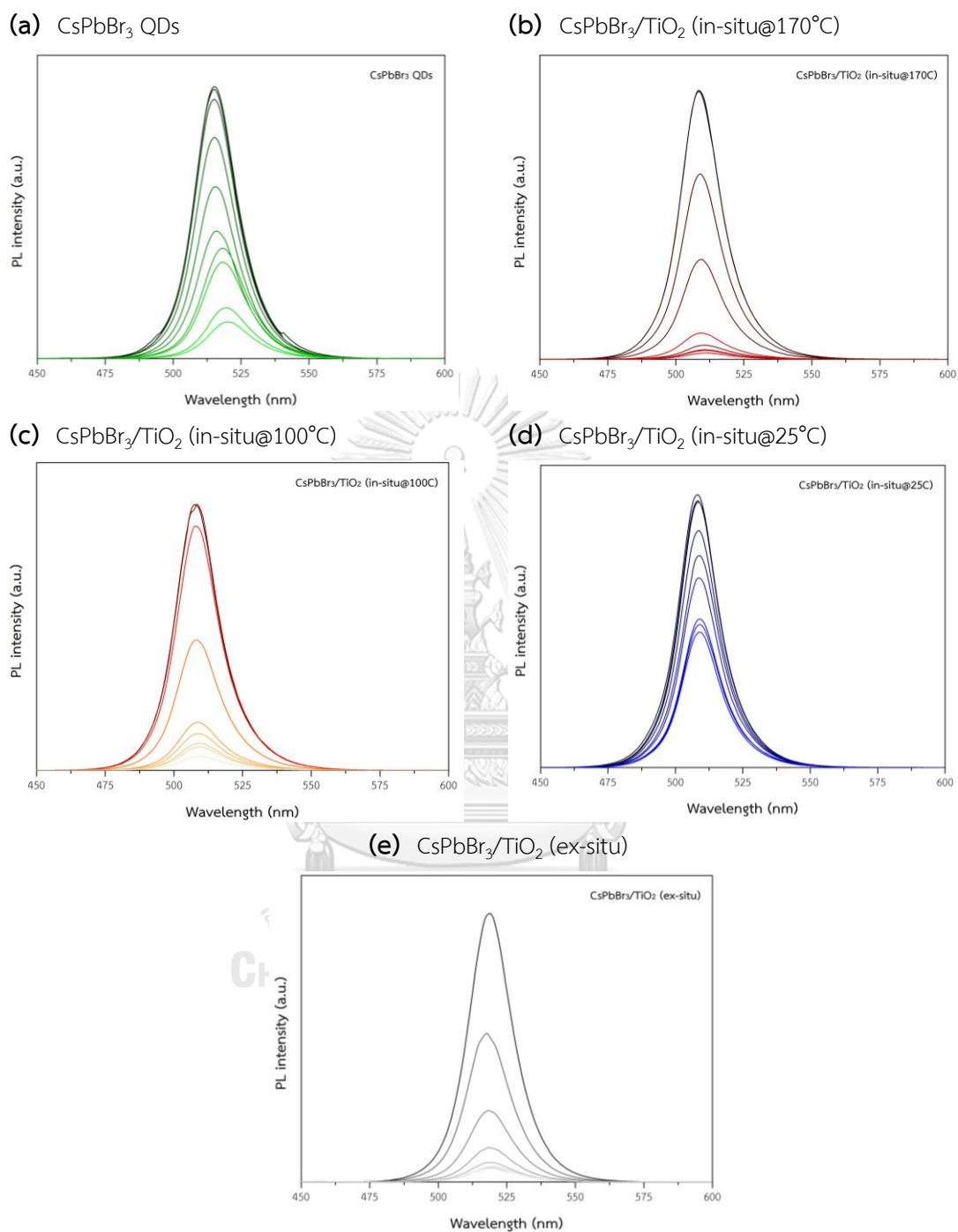


Figure 4.20 Photostability of CsPbBr₃ QDs, CsPbBr₃/TiO₂ coated by in-situ method at 170°C, 100°C, 25°C and by ex-situ method under light illumination at 455 nm.

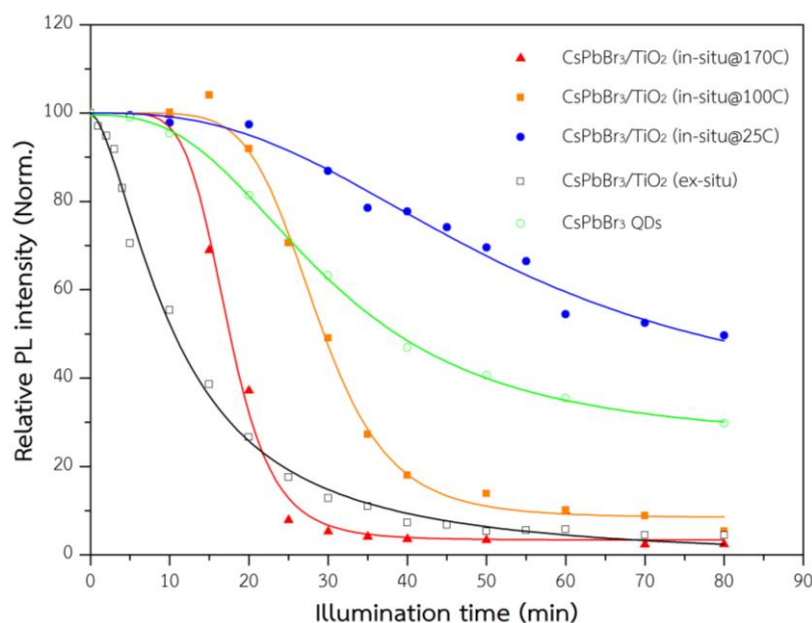


Figure 4.21 The comparison of relative PL intensity for the five samples which were dispersed in toluene and continuously soaked visible light source at 455 nm.

4.5 Photoelectrochemical characterizations

In order to investigate the efficiency of CsPbBr₃/TiO₂ coated by various method for the further application, the photoelectrochemical characterizations have been used to test the charge transport properties of CsPbBr₃ QDs after coating with TiO₂ [2]. The cyclic voltammetry (CV) measurement with potentials scanned between -1.7 and 1.7 V was carried out with a standard three-electrode setup by using FTO as a working electrode, a Pt mesh as a counter electrode and Ag/AgNO₃ wire as a reference electrode. The bare CsPbBr₃ QDs showed the oxidation peak at 1.28 V and the reduction peak at -1.37 V (figure 4.23a) corresponding to the previous study [31]. However, the oxidation of CsPbBr₃ QDs should display the second peak at 0.8 V since the CsPbBr₃ QDs in solution could not completely contact to the electrode, while the previous study directly coated CsPbBr₃ QDs on the FTO. The CsPbBr₃/TiO₂ displayed two anode peaks at 0.08 V and 0.69 V for in-situ@170°C (figure 4.23b), 0.06 V and 0.88 V for in-situ@100°C (figure 4.23c), 0.13 V and 0.91 V for in-situ@25°C (figure 4.23d) and 0.21 V and 0.97 V for ex-situ (figure 4.23e). Interestingly, compared with bare CsPbBr₃ QDs, the CsPbBr₃/TiO₂ exhibited two oxidation peaks at lower potentials

and much higher current because the CsPbBr₃ QDs could be easily oxidized to positive charge of CsPbBr₃ QDs⁺ [9] after coating with TiO₂. However, the reduction peaks cannot be identified clearly for the CsPbBr₃/TiO₂ samples.

Then, the current-voltage (IV) curves were performed by using three-electrode system with two-compartments separated by nafion membrane, where methanol was used as an electron donor and POM was used as an electron acceptor. When observed the IV curve of photoelectrochemical cell at low applied bias (figure 4.22), it was found that the current of the samples increased as the first oxidation potential decreased. For example, the in-situ@100°C sample had the lowest oxidation potential (0.06 V) so it showed the highest current. In contrast, the bare CsPbBr₃ QDs had the highest oxidation potential (1.28 V) so it showed the lowest current. Therefore, the TiO₂ could increase charge transfer of CsPbBr₃ QDs by injecting electrons to its CBM resulting in the higher current of all CsPbBr₃/TiO₂ samples compared to bare CsPbBr₃ QDs. Moreover, the in-situ coated sample at 100°C exhibited the best performance in this electrochemical cell, even though its stability was not the highest. However, the enhancement of charge transfer property was not directly consistent with the amount of TiO₂ on QDs surface since the structural and optical properties after encapsulation process also affected the QDs performance.

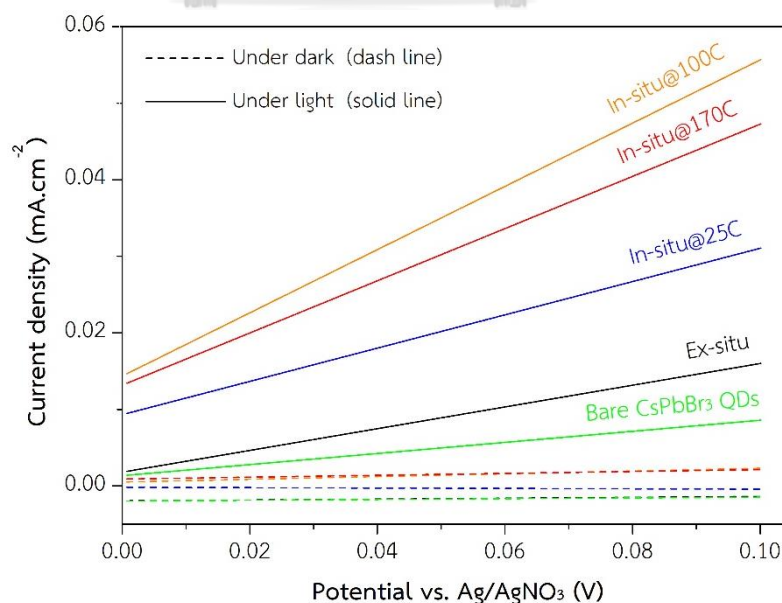


Figure 4.22 The comparison of IV curves for the five samples in PEC cell (FTO (s) | QDs solution, 0.12 M Methanol || POM | Pt (s)).

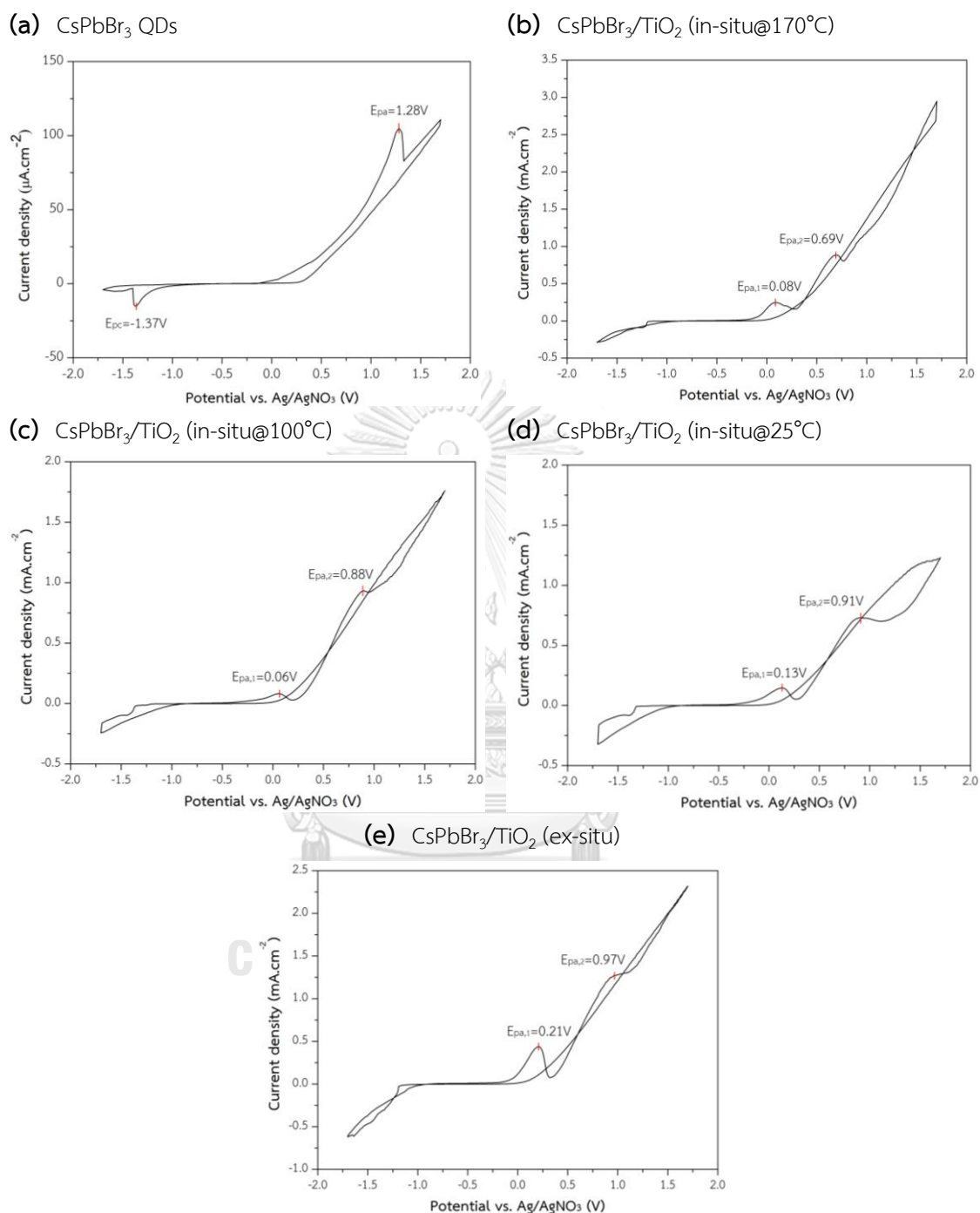


Figure 4.23 CV curves recorded during the oxidation and reduction of five samples in 0.1 M TBAPF₆/Acetonitrile with 10 mV.s⁻¹ sweep rate (FTO (s) | QDs solution | Pt (s)).

CHAPTER 5

CONCLUSION

5.1 Conclusions

1. CsPbBr₃ QDs were successfully synthesized via hot-injection and encapsulated with TiO₂ via in-situ method and ex-situ method. The encapsulation process had an influence on morphology, structural and optical properties as well as the compositional ratio of Ti on the surface.
 - 1.1 The morphology of in-situ coated samples was in a cubic shape with the average size of 11 - 14 nm. While ex-situ coated sample was aggregated as clusters with the average size of 200-540 nm.
 - 1.2 The structure of CsPbBr₃/TiO₂ was orthorhombic. The growth of (112) face was hindered at higher TTIP injection temperature.
 - 1.3 The PLQY (bandgap) was 98.5% (2.39 eV), 93.5% (2.35 eV), 80.6% (2.39 eV), 72.1% (2.39 eV) and 1.3% (2.33 eV) for bare CsPbBr₃ QDs, in-situ coated sample at 170°C, 25°C and 100°C, and ex-situ coated sample, respectively.
 - 1.4 The compositional ratio of Ti to Cs was 0.02, 0.15, 0.10 and 3.50 for in-situ coated samples at 170°C, 100°C and 25°C, and ex-situ coated sample, respectively.
2. CsPbBr₃/TiO₂ synthesized via in-situ method, in which the temperature of titanium precursor injection was 25°C, exhibited less defects on (112) face and large amount of Ti (Cs : Ti ratio 1 : 0.10) resulting in the excellent stability under ambient air (93%, 5 days), in toluene (80%, 7 days), in DIW (48%, 30 min) and under light illumination (48%, 80 min) since TiO₂ can act as a protecting shell of CsPbBr₃ QDs from the degradation by these factors.
3. Encapsulation of CsPbBr₃ QDs with TiO₂ was proved by PEC that TiO₂ can improve charge transfer of CsPbBr₃/TiO₂. The in-situ coated sample at 100°C exhibited the best charge transport property due to the lowest oxidation potential at 0.06 V which resulted in the highest current.

5.2 Recommendations for the future work

1. Investigate the stability of CsPbBr₃/TiO₂ during applying in the applications such as the effects of applied bias in optoelectronic devices on their structural properties and test the performance in other applications such as solar cell, etc.
2. Characterize crystallographic structure of materials at an atomic scale by high-resolution transmission electron microscopy in order to clarify the effects of TiO₂ encapsulation on the structure of CsPbBr₃ QDs.



REFERENCES

- [1] Yang F, Kapil G, Zhang P, Hu Z, Kamarudin MA, Ma T, et al. Dependence of Acetate-Based Antisolvents for High Humidity Fabrication of CH₃NH₃PbI₃ Perovskite Devices in Ambient Atmosphere. *ACS Applied Materials & Interfaces*. 2018;10(19):16482-9.
- [2] Li ZJ, Hofman E, Li J, Davis AH, Tung CH, Wu LZ, et al. Photoelectrochemically Active and Environmentally Stable CsPbBr₃/TiO₂ Core/Shell Nanocrystals. *Adv Funct Mater*. 2018;28(1):1704288.
- [3] Sievers NV, Pollo LD, Corção G, Medeiros Cardozo NS. In situ synthesis of nanosized TiO₂ in polypropylene solution for the production of films with antibacterial activity. *Mater Chem Phys*. 2020;246:122824.
- [4] Zhong Q, Cao M, Hu H, Yang D, Chen M, Li P, et al. One-Pot Synthesis of Highly Stable CsPbBr₃@SiO₂ Core-Shell Nanoparticles. *ACS Nano*. 2018;12(8):8579-87.
- [5] Imran M, Caligiuri V, Wang M, Goldoni L, Prato M, Krahn R, et al. Benzoyl Halides as Alternative Precursors for the Colloidal Synthesis of Lead-Based Halide Perovskite Nanocrystals. *J Am Chem Soc*. 2018;140(7):2656-64.
- [6] Mertens R. Perovskite Introduction 2018 [updated 28/04/2018]. Available from: <https://www.perovskite-info.com/perovskite-introduction>.
- [7] Tai Q, Tang K-C, Yan F. Recent progress of inorganic perovskite solar cells. *Energy & Environmental Science*. 2019;12(8):2375-405.
- [8] Grätzel M. Photovoltaic and photoelectrochemical conversion of solar energy. *Philosophical Transactions of the Royal Society A: Mathematical, Physical and Engineering Sciences*. 2007;365(1853):993-1005.
- [9] Wang X-Y, Wu M-X, Ding S-N. Anodic electrochemiluminescence from CsPbBr₃ perovskite quantum dots for an alkaline phosphatase assay. *Chem Commun (Camb)*. 2020;56(58):8099-102.
- [10] Kumar S, Ahirwar S, Satpati AK. Insight into the PEC and interfacial charge transfer kinetics at the Mo doped BiVO₄ photoanodes. *RSC Advances*. 2019;9(70):41368-82.

- [11] Band Gap and Semiconductor Current Carriers 2018 [updated 07/09/2018. Available from: <https://www.circuitbread.com/tutorials/band-gap-and-semiconductor-current-carriers>.
- [12] Ltd. O. Perovskites and Perovskite Solar Cells 2018 [Available from: <https://www.ossila.com/pages/perovskites-and-perovskite-solar-cells-an-introduction>.
- [13] Boyd CC, Cheacharoen R, Leijtens T, McGehee MD. Understanding Degradation Mechanisms and Improving Stability of Perovskite Photovoltaics. *Chem Rev.* 2019;119(5):3418-51.
- [14] Byranvand MM, Kharat AN, Taghavinia N. Moisture stability in nanostructured perovskite solar cells. *Mater Lett.* 2019;237:356-60.
- [15] Pearson AJ, Eperon GE, Hopkinson PE, Habisreutinger SN, Wang JT-W, Snaith HJ, et al. Oxygen Degradation in Mesoporous Al₂O₃/CH₃NH₃PbI₃-xCl_x Perovskite Solar Cells: Kinetics and Mechanisms. *Advanced Energy Materials.* 2016;6(13):1600014.
- [16] deQuilettes DW, Zhang W, Burlakov VM, Graham DJ, Leijtens T, Osherov A, et al. Photo-induced halide redistribution in organic-inorganic perovskite films. *Nature Communications.* 2016;7(1):11683.
- [17] Noh JH, Im SH, Heo JH, Mandal TN, Seok SI. Chemical Management for Colorful, Efficient, and Stable Inorganic-Organic Hybrid Nanostructured Solar Cells. *Nano Lett.* 2013;13(4):1764-9.
- [18] Kulbak M, Gupta S, Kedem N, Levine I, Bendikov T, Hodes G, et al. Cesium Enhances Long-Term Stability of Lead Bromide Perovskite-Based Solar Cells. *The Journal of Physical Chemistry Letters.* 2016;7(1):167-72.
- [19] Saidaminov MI, Kim J, Jain A, Quintero-Bermudez R, Tan H, Long G, et al. Suppression of atomic vacancies via incorporation of isovalent small ions to increase the stability of halide perovskite solar cells in ambient air. *Nature Energy.* 2018;3(8):648-54.
- [20] Wang K, Jin Z, Liang L, Bian H, Bai D, Wang H, et al. Publisher Correction: All-inorganic cesium lead iodide perovskite solar cells with stabilized efficiency beyond 15%. *Nature Communications.* 2018;9(1):4935.

- [21] Hirotsu S, Harada J, Iizumi M, Gesi K. Structural Phase Transitions in CsPbBr₃. *J Phys Soc Jpn.* 1974;37(5):1393-8.
- [22] Zhang M, Zheng Z, Fu Q, Chen Z, He J, Zhang S, et al. Growth and characterization of all-inorganic lead halide perovskite semiconductor CsPbBr₃ single crystals. *CrystEngComm.* 2017;19(45):6797-803.
- [23] Rahimi N, Pax RA, Gray EM. Review of functional titanium oxides. I: TiO₂ and its modifications. *Prog Solid State Chem.* 2016;44(3):86-105.
- [24] Guo Z, Ambrosio F, Pasquarello A. Hole diffusion across leaky amorphous TiO₂ coating layers for catalytic water splitting at photoanodes. *Journal of Materials Chemistry A.* 2018;6(25):11804-10.
- [25] Sun S, Song P, Cui J, Liang S. Amorphous TiO₂ nanostructures: synthesis, fundamental properties and photocatalytic applications. *Catalysis Science & Technology.* 2019;9(16):4198-215.
- [26] Zheng Z, Liu L, Yi F, Zhao J. Significantly improving the moisture-, oxygen- and thermal-induced photoluminescence in all-inorganic halide perovskite CsPbI₃ crystals by coating the SiO₂ layer. *J Lumin.* 2019;216:116722.
- [27] Pramata AD. Photoinduced Electron Transfer in Semiconductor Nanocrystal/Polyoxometalate Systems and Its Application for Electron Storage, Luminescence Mechanism Analysis, and Photoemission Switching. Kumamoto University: Kumamoto University; 2019.
- [28] Moyer E, Kanwat A, Cho S, Jun H, Aad R, Jang J. Ligand removal and photo-activation of CsPbBr₃ quantum dots for enhanced optoelectronic devices. *Nanoscale.* 2018;10(18):8591-9.
- [29] Chen J, Liu D, Al-Marri MJ, Nuuttila L, Lehtivuori H, Zheng K. Photo-stability of CsPbBr₃ perovskite quantum dots for optoelectronic application. *Sci China Mater.* 2016;59(9):719-27.
- [30] Ellis JL, Hickstein DD, Schnitzenbaumer KJ, Wilker MB, Palm BB, Jimenez JL, et al. Solvents Effects on Charge Transfer from Quantum Dots. *J Am Chem Soc.* 2015;137(11):3759-62.

- [31] Samu GF, Scheidt RA, Kamat PV, Janáky C. Electrochemistry and Spectroelectrochemistry of Lead Halide Perovskite Films: Materials Science Aspects and Boundary Conditions. Chem Mater. 2018;30(3):561-9.



REFERENCES



จุฬาลงกรณ์มหาวิทยาลัย
CHULALONGKORN UNIVERSITY

VITA

NAME Parina Nukett

DATE OF BIRTH 13 February 1996

PLACE OF BIRTH Bangkok, Thailand

INSTITUTIONS ATTENDED B.Eng., Department of Chemical Engineering, Faculty of Engineering, King Mongkut's Institute of Technology Ladkrabang, Thailand, 2017.
M.Eng., Center of Excellence in Particle Technology, Department of Chemical Engineering, Faculty of Engineering, Chulalongkorn University, Thailand, 2019.

HOME ADDRESS 12/21 Chalongkrung Road, Tabyao Sub-district, Ladkrabang District, Bangkok 10520 Thailand.